Traffic 2013; **14:** 440–457

doi:10.1111/tra.12040

Proteomic Analysis of Clathrin Interactions in Trypanosomes Reveals Dynamic Evolution of Endocytosis

Vincent O. Adung'a[1,2], Catarina Gadelha[1] and Mark C. Field[1,*]

[1] *Department of Pathology, University of Cambridge, Tennis Court Road, Cambridge CB2 1QP, UK*
[2] *Department of Biochemistry and Molecular Biology, Egerton University, P.O. Box 536 Egerton, Kenya*

**Corresponding author: Mark C. Field, mcf34@cam.ac.uk*

Endocytosis is a vital cellular process maintaining the cell surface, modulating signal transduction and facilitating nutrient acquisition. In metazoa, multiple endocytic modes are recognized, but for many unicellular organisms the process is likely dominated by the ancient clathrin-mediated pathway. The endocytic system of the highly divergent trypanosomatid *Trypanosoma brucei* exhibits many unusual features, including a restricted site of internalization, dominance of the plasma membrane by GPI-anchored proteins, absence of the AP2 complex and an exceptionally high rate. Here we asked if the proteins subtending clathrin trafficking in trypanosomes are exclusively related to those of higher eukaryotes or if novel, potentially taxon-specific proteins operate. Co-immunoprecipitation identified twelve *T. brucei* clathrin-associating proteins (TbCAPs), which partially colocalized with clathrin. Critically, eight TbCAPs are restricted to trypanosomatid genomes and all of these are required for robust cell proliferation. A subset, TbCAP100, TbCAP116, TbCAP161 and TbCAP334, were implicated in distinct endocytic steps by detailed analysis of knockdown cells. Coupled with the absence of orthologs for many metazoan and fungal endocytic factors, these data suggest that clathrin interactions in trypanosomes are highly lineage-specific, and indicate substantial evolutionary diversity within clathrin-mediated endocytosis mechanisms across the eukaryotes.

Key words: clathrin, endocytosis, intracellular transport, LECA, molecular evolution, protein interaction networks, trypanosoma

Received 20 September 2012, revised and accepted for publication 7 January 2013, uncorrected manuscript published online 10 January 2013, published online 5 February 2013

Membrane trafficking is essential for nutrient uptake, regulation of signal transduction, receptor expression and control, maintenance of cell polarity, antigen presentation and parasite virulence mechanisms among other functions (1–4). The best-characterized endocytic pathway involves the coat protein clathrin, but additional mechanisms are known for metazoan cells. Endocytosis can thus be defined as either clathrin-mediated endocytosis (CME) (5–7) or clathrin-independent (2,8,9); examples of the latter include RhoA-dependent, cdc42-dependent, Arf6-dependent and caveolin-dependent pathways (9). Comparative genomics suggests that clathrin is an ancient feature of eukaryotes (10), as the protein is present in all modern supergroups and hence likely also present in the last eukaryotic common ancestor (LECA), while the key proteins defining clathrin-independent pathways, where known, appear to be lineage-specific, and therefore are inferred as innovations that came post-LECA (10). In unicellular pathogens, the plasma membrane and the endo/exocytic system also represent the principal interface with the host and contribute to immune evasion, host cell invasion and defense, all vital processes for the effective infection and persistence of many pathogens, including *Plasmodium*, *Toxoplasma*, pathogenic fungi and trypanosomes (3,4).

Trypanosoma brucei is a flagellate protozoan and the causative agent of sleeping sickness in humans and n'agana in cattle. The parasite is responsible for severe morbidity and mortality, significantly limiting human economic activities in sub-Saharan Africa. Related organisms cause a spectrum of morbidities including Chagas' disease in South America and Kala Azar in Asia, and combined have an impact that encompasses much of the globe. *Trypanosoma brucei* infections are characterized by the chronic presence of the parasite within the bloodstream and lymphatic systems. To evade immune clearance, bloodstream form parasites (BSFs) undergo antigenic variation by sequential expression of antigenically distinct glycosyl-phosphatidylinositol (GPI)-anchored variant surface glycoproteins (VSG; (11,12)). By contrast, in the insect vector, the major proliferative procyclic form (PCF) expresses an invariant protease-resistant GPI-anchored protein, procyclin (13). The two life stages are marked by significant morphological, structural and biochemical changes, and of particular relevance is the developmental regulation of endocytosis, estimated at ~20-fold higher in BSF than PCF (3).

The endocytic system of *T. brucei* has been comparatively well studied, and many protein participants are now known. The endomembrane system is extremely polarized, with most organelles of the exo- and endocytic pathways located at the posterior cell pole, while exchange with the plasma membrane is restricted to the flagellar pocket (FP), an invagination at the base of the flagellum. Rapid endocytosis in BSFs contributes to immune defense by efficient recycling of VSG and fast

Traffic

turnover of invariant surface proteins, both of which likely contribute to clearance of surface bound antibodies (14,15). All *T. brucei* endocytosis is clathrin mediated (16), but the AP-2 adaptin complex, a hallmark of plasma membrane clathrin recruitment and cargo selection in most organisms, is absent (17). Important proteins include several Rab GTPases (18–22), ADP-ribosylation factor 1 (ARF1) (23), clathrin (16,24), actin (25) and myosin (26), and the importance of ubiquitylation in sorting and internalization has recently been demonstrated (15,27), while the process appears dynamin-independent (28). However, orthologs of a number of critical endocytic proteins have not been identified; while this may reflect extreme sequence divergence, it is also possible that the failure to identify these genes reflects true absence (29).

In trypanosomes, surface proteins are packed into clathrin-coated pits (CCPs) that undergo scission into ~135 nm diameter clathrin-coated vesicles (CCVs) (24). TbEpsinR, the only characterized trypanosome endocytic clathrin adaptor to date, has limited involvement in bulk membrane internalization, *albeit* with a general role in membrane protein endocytosis (30). The CCVs shed their clathrin coat and subsequently dock and fuse with Rab5 early endosomes. Cargo are sorted and packaged into 50–60 nm diameter CCVs (24,31), but VSG is concentrated into disk-like Rab11-positive exocytic structures that subsequently fuse with the FP (24,32–34,19). Clathrin is associated with the membranes of the FP/sorting endosomes and also the *trans*-Golgi cisterna (35,24), an indication that the clathrin interaction network is likely complex and participates in multiple pathways.

Despite this level of understanding, it is unclear if the failure to detect endocytic protein genes in the trypanosome genome represents a secondary reduction accompanying a parasitic lifestyle, or reflects deep evolutionary divergence between trafficking mechanisms of the different eukaryotic supergroups, and the major proteins required to recruit clathrin to the FP membrane and other organelles remain unknown. Given the prominent role that the FP plays both in trafficking and as part of the spatial organization of organelles in many trypanosomatids, this is a crucial gap in understanding. Demonstration by RNAi of endocytic essentiality *in vivo* suggests these pathways offer therapeutic possibilities, while a recent phenocopy using chemical biology suggests that this may well be exploitable (16,36).

Here we used co-immunoprecipitation (co-IP), mass spectrometry (MS) proteomics, genomic *in situ*-tagging, immunofluorescence and electron microscopy to identify and validate a cohort of trypanosome clathrin-associating proteins (TbCAPs). Functional analysis of a subset of TbCAPs confirmed roles in clathrin-mediated trafficking. Remarkably, many TbCAPs appear to be restricted to the trypanosomatids, suggesting considerable evolutionary divergence in clathrin-mediated transport mechanisms across taxa.

Results

Identification of candidate clathrin-interaction partners

As few candidate interaction partners for clathrin have been identified in trypanosomes using *in silico* approaches (10), we chose a proteomics-based strategy to potentially uncover both conserved and novel clathrin-associated proteins. Strategies comparing knockout or knockdown cells, as successfully exploited in metazoan cells, were not available to us due to the essentiality of the clathrin-mediated endocytic pathway (37). Co-immunoprecipitations using polyclonal antibody rabbit anti-clathrin heavy chain (anti-TbCHC) on equivalent amounts of BSF and PCF cell lysates were performed (35). The antibody was incubated with cell lysates and antibody-antigen complexes isolated by binding to Protein A sepharose beads. To monitor non-specific binding, equivalent preparations using beads plus lysate, and beads plus antibody alone were analyzed. The immunoprecipitates were resolved by SDS-PAGE and visualized by silver-staining (Figure 1). In both BSF and PCF lysates (lanes 3 and 4, respectively), multiple bands were detected, suggesting co-immunoprecipitation. Similar profiles were observed in three independent co-immunoprecipitations, indicating that the isolation procedure was reproducible. Further, the profile similarity suggests the compositions of the immuno-isolations are broadly similar in both life cycle stages. The prominent ~175 kDa band was identified as TbCHC by MS (Figure 1; Table 1). As expected, the gel band representing TbCHC was of higher intensity in BSF than PCF, in agreement with developmental regulation of clathrin and endocytic activity (35,38), and the increased recovery of co-immunoprecipitated proteins in the BSF compared to PCF pullouts suggests developmental regulation of other members of the putative interactome. Note that candidate interacting partners all appear to be substoichiometric when compared to clathrin; this may reflect promiscuity of clathrin interactions and is similar to the stoichiometry observed from classical isolations of clathrin coated vesicles from multiple mammalian sources (39). We chose to pursue the BSF isolation as higher protein quantities were recovered, while the essentiality of endocytosis in this life cycle stage 3, together with observations that many endocytic components are lethal upon ablation in BSF (e.g. actin (25) and myosin (26)), suggests that the BSF clathrin endocytic complexes are potentially better candidates for therapeutic intervention. The precise configuration of the clathrin-partner complexes isolated is unknown as no specific steps were taken to preserve clathrin lattices, or to disassemble them; it is probable that the IP represents a mixture of clathrin states. Further, we are aware that the IP conditions are comparatively stringent, and therefore we expect that we are sampling a subset of the full clathrin-interaction protein cohort.

Liquid chromatography tandem mass spectrometry (LC/MS/MS) was performed on gel fragments migrating above the Ig heavy chain band (≥60 kDa; Figure 1B) from

Table 1: Accession numbers and annotations of putative clathrin-associating proteins identified from MS. The accession numbers, annotation, predicted domains and calculated molecular weights were determined from public genome and protein databases

Gene id	Annotation	Score (no. peptides) [I][II][III]	Domains/comments	Size (kDa)	Name
Tb927.10.6050	CHC (Clathrin Heavy Chain)	[51(9);1109(34); 40(7)][1540(31);2850(66); 810(18);523(11); 162(2)] [196(3)]		190	TbCHC
Tb11.01.3110	Hsc70	[1024(23);249(7);229(4)][98(5)]	Hsc70	75	TbHsc70
Tb927.4.3380	Myosin 1B (58)	[36(3)]	Myosin head, WW, TH1, 131 Zinc-Finger-FYVE/ PHD-type (26)		TbMyo1
Tb927.6.3500	TbRME-8	[37(4)]	DnaJ	254	TbRME8
Tb927.7.4960	Hypothetical	[31(2)][22(1);24(2);24(1); 24(1); 24(1)]		50	TbCAP50
Tb927.5.2660	Hypothetical	[30(1);32(2);37(1);30(3)]	SDA1/NUC130/3NT domain	99	TbCAP99
Tb927.10.2130	Hypothetical	[30(7);30(5)][24(3);21(3);21(1)]	Vps51/67	100	TbCAP100
Tb09.211.0480	Hypothetical	[38(5);30(3);29(3)][20(3)]		125	TbCAP125
Tb11.01.5850	Hypothetical	[30(3)][36(1)][22(2)]	WD40	116	TbCAP116
Tb927.10.720	Hypothetical	[42(4);][39(3);37(3);36(1)]	PB1	118	TbCAP118
Tb927.7.3930	Hypothetical	[32(3)][22(2)]		161	TbCAP161
Tb927.1.4520	Hypothetical	[30(4)][21(2)]	Zinc finger, RING-type	83	
Tb11.02.4760	Hypothetical	[33(4);44(5)][24(3)]		186	TbCAP186
Tb927.10.4170	Hypothetical	[42(4);48(9);47(5);44(4)] [33(2)32(1)] [25(3);29(3)]		292	TbCAP292
Tb09.244.2600	Ankyrin-repeat protein, putative	[43(5)][27(18);25(15);31(1)]	Ankyrin	334	TbCAP334
Tb927.4.800	Hypothetical	45(18);32(12)][31(9);22(2)]	PDZ, HEAT, FATC domain Armadilo fold, PIK-related kinase, Rapamycin binding domain.	291	TbTORL1
Tb927.10.8420	PI3K, putative	[33(4);34(4);30(6);34(1)] [31(1)34(1)]	Similar to TbTOR3 minus PDZ	271	TbTOR1
Not analyzed					
Tb11.02.1000	Hypothetical	[32(3);29(3)][23(2)]	Peptidyl-prolyl *cis-trans* isomerase, FKBP-type	92	
Tb927.7.4940	Oligopeptidase B protein, putative	[38(3)][39(6)][24(2);24(6)]	Prolyloligopeptidase family	104	
Tb10.61.1020	Kinesin, putative	[40(4)][21(3);22(2)]	Kinesin motor	124	
Tb927.8.7590	Receptor-type adenylate	[38(14);50(8);45(3)][45(3)]	Calcium-binding EF-hand	140	
	Adenylate/Guanylate cyclase cyclase GRESAG 4, putative	[20(3);37(6);22(4)]			
Tb927.7.920	Dynein heavy chain, putative	[32(6)][21(4)]	Dynein heavy chain, AAA + ATPase	468	
Tb927.7.3160	Dynein heavy chain,	[31(6);47(9);65(11)] [33(7)][23(5)]	Dynein heavy chain, AAA + ATPase cytosolic, putative	597	
Tb927.1.1740	Hypothetical	[54(2);44(2);31(3);38(2)][28(1); 27(1);31(2);31(1)][19(1); 23(4);25(2)]	Concanavalin A-like lectin/glucanase	811	
Tb11.01.0010	DNA polymerase kappa, putative	Members of the family occurred multiple times	Probable nonspecific hit		

Each square bracket represents the score value of an independent MS experiment. The number of peptides recovered for each predicted protein is in curved brackets. The names assigned to the putative clathrin-associating proteins (TbCAPs) based on predicted molecular weight are shown in the far right column. See Table S1 for raw data.

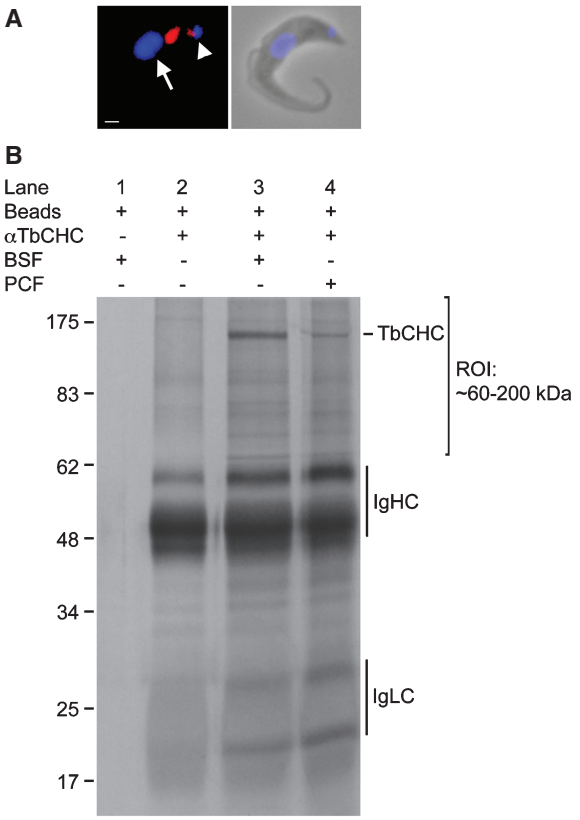

Figure 1: Immunoprecipitation of clathrin-interacting proteins (TbCAPs). A) Immunofluorescence localization of clathrin (red) to the endocytic region between the DAPI (blue) stained kinetoplast (arrowhead) and nucleus (arrow). Scale bar = 1 μM. B). Protein complexes isolated by immunoprecipitation from BSF and PCF lysates using rabbit anti-clathrin heavy chain (TbCHC) antibody were resolved on 12% SDS-PAGE. Beads plus lysate or antibody alone were used as control. Silver staining of gels showed the presence of the ~175 kDa TbCHC fragment in BSF (lane 3) and PCF (lane 4) but not in the controls (lanes 1 and 2). BSF gel fragments above the antibody heavy chain (IgHC) in the range of ~60–200 kDa were subjected to MS (ROI; region of interest). The gel is a representative of multiple replicates.

three independent BSF co-immunoprecipitations. The region migrating faster than the immunoglobulin heavy chain was excluded as several proteins were observed in the antibody plus bead control lane. Peptide sequences predicted by MS were used to query the *T. brucei* predicted proteome to identify candidate clathin-associated proteins (TbCAPs). To select candidate TbCAPs for further investigation, we applied the following criteria: (i) identification of the open reading frame (ORF) in two or more independent experiments, (ii) highly significant identification from multiple peptides, (iii) orthology to proteins from other organisms implicated in trafficking, (iv) the presence of domains involved in trafficking and/or protein–protein interactions and (v) predicted molecular weight within or close to the analyzed gel region. An occurrence in multiple analyses was accorded a higher weighting. A schematic representation of the experimental strategy is shown in Figure S1, Supporting Information. We rejected proteins known to frequently contaminate proteomic data, that were confidently assigned as functioning elsewhere or have extremely high abundance and lack additional evidence to support an assignment as a TbCAP (40). This conservative strategy is likely to under-sample highly novel gene products.

The trypanosome clathrin interactome contains many novel proteins

Besides TbCHC (Tb927.10.6050), over 20 proteins were confidently identified (Table 1). TbCHC had the highest score and was recovered from all three experiments, as was the product of Tb11.01.3110 (TbHsc70), the ortholog of the clathrin uncoating ATPase of higher eukaryotes. The ORF Tb927.4.3380, which encodes myosin IB (TbMyo1) and is involved in endocytosis (26), as well as the ortholog of metazoan RME8 (Tb927.6.3500), which is involved in recycling of endocytic proteins (41), were both recovered from one of three independent experiments. No clathrin uncoating proteins or proteins homologous to auxilin for example were found; however for the latter there is no ortholog in the genome.

Three proteins implicated in target of rapamycin (TOR) signaling pathways, Tb927.10.8420 (TbTOR1), Tb927.4.800 (TbTORL1) and Tb927.4.420 (TbTOR2) (42,43) were also isolated, although TbTOR2 was retrieved only once. A kinesin encoded by Tb927.10.15390, a member of kinetoplastid-specific X1 family was recovered thrice (44,45). Tb927.7.920 and Tb927.7.3160 encode axonemal and cytosolic dynein heavy chains respectively (46). Some of the proteins recovered multiple times are probable contaminants, e.g. nucleic acid modifying proteins, although interactions with clathrin and involvement in mitosis, as recently reported for higher eukaryotes (47,48) cannot be ruled out. Candidate TbCAPs encoded by Tb11.01.5850, Tb927.10.720, Tb927.10.2130, Tb09.211.0480, Tb927.10.4170, Tb11.02.4760, Tb927.7.4960, Tb927.7.3930, Tb927.1.1740 and Tb09.244.2600 all encode hypothetical proteins. Overall, the identification of several known clathrin-interacting proteins suggests that the analysis also identified new putative clathrin-associated proteins. However, some proteins known to bind clathrin, for example TbEpsinR, (30) were not returned, indicating under-sampling. This is likely a result of stringent conditions used for the cell lysis and IP.

Several TbCAPs locate to the endomembrane region

Clathrin localizes to structures restricted to the region between the kinetoplast (the region of the trypanosome single mitochondrion that concentrates all mtDNA) and nucleus (Figure 1A). Therefore, we anticipated that *bona fide* TbCAPs should localize to this region or part thereof, reflecting association with clathrin. We determined the locations of TbCAPs by expression of hemagglutinin (HA), FLAG or GFP epitope-tagged versions of the proteins, and verified that the tagged proteins were of the correct apparent molecular weights (Figures 2, S2 and S3). Twelve

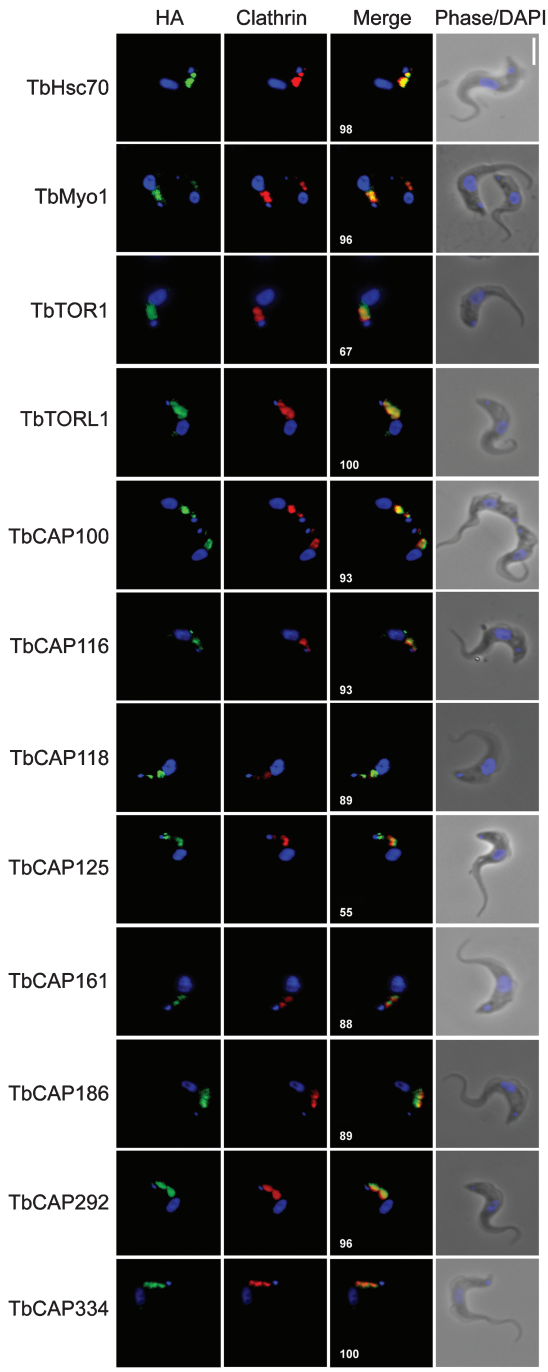

Figure 2: Localization of TbCAP candidates. Ectopic expression of candidate TbCAPs fused to a C-terminal HA tag in the pXS5 vector or endogenous-locus tagged at the C-terminus was performed and correct integration confirmed by western blot or PCR. Subsequently, TbCAP localization with anti-HA (green), anti-TbCHC (red) and DAPI (blue) was performed. All twelve TbCAP candidates shown here co-localize with clathrin in the region between the kinetoplast and nucleus, suggesting involvement in endomembrane dynamics. The frequency of cells in which clear co-localization was observed are shown in white (percent). Scale bar (top right) = 1 μM.

HA-tag candidates localized in the region between the nucleus and the kinetoplast, and their signal distribution overlapped with clathrin (Figure 2). A similar localization was observed with FLAG- and GFP-tagged proteins (Figure S2) indicating that the localization is likely authentic. This group includes TbHsc70 and TbMyo1, TbCAP100, TbCAP116, TbCAP118, TbCAP125, TbCAP161, TbCAP 186, TbCAP334, TbCAP292, TbTOR1 and TbTOR-L1. The gene product of Tb927.5.2660 (TbCAP99) localized in the nucleolus, while that of Tb927.7.4960 (TbCAP50) was inconclusive (Figure S2). TbTOR1 and TbTORL1 were reported to localize at the nucleus and cytosolic granules by other investigators based on polyclonal antibody staining, and the localizations observed here are inconsistent. Further work is required to resolve this issue and TbTOR1 and TbTORL1 were not investigated further (42,43). Ten out of twelve TbCAP candidates are novel proteins that co-IP with TbCHC and display overlapping locations with clathrin in the posterior region of the cell, suggesting *bona fide* clathrin association.

Comparative genomics of TbCAP proteins

Trypanosomes are among the most divergent of eukaryotic organisms, and may even lie close to the eukaryotic root (49–51). Evolutionary investigations in *T. brucei* demonstrate the absence of many widely conserved endocytic factors, including AP-2, epsin and Eps15 (10). To investigate the evolutionary representation of the TbCAPs, BLAST (52), PSI-BLAST (53), HMMER (54) and reciprocal best BLAST searches were performed to identify orthologs and domain architectures that may be informative of function (see *Methods*) (Figure 3). For candidate orthologs, CLUSTALW alignment (55) was used to inspect sequence and domain organization conservation.

With the exceptions of TbHsc70, TbTOR1 and 2, TbMyoI and TbCAP100, TbCAPs appear restricted to the trypanosomatids (Figure 3). The conservation of Hsc70 has been reported previously (56), while Serfontein et al. (57) described conservation of most components of the TSC1/TSC2-TOR signaling pathway, including TOR1. Interestingly, the PDZ domain-containing TOR kinase named TORL1 represents a trypanosomatid-specific form and a third TOR kinase, also recently suggested as involved in acidocalcisome function (43). Trypanosomatids have only two myosin families, namely IB and XXI (58,59), and TbMyoI appears to function in endocytosis (26). TbMyoI is part of the myosin I family, and representatives are present in fungi, amoeba, worms, flies and other eukaryotes but absent from Viridiplantae and alveolates (60,58,61). TbCAP100 contains a Vps51/67 domain which is present in many supergroups; TbCAP100 is homologous to *Homo sapiens* Ang2 and *Saccharomyces cerevisiae* Vps51 (62), and hence represents a trypanosome Vps51 ortholog not identified in an earlier *in silico* study (63).

The members of nutrient-sensing TOR signaling network – namely TbTOR1, TbTORL1 and TbTOR2 – have a similar domain organization, except for an extra domain

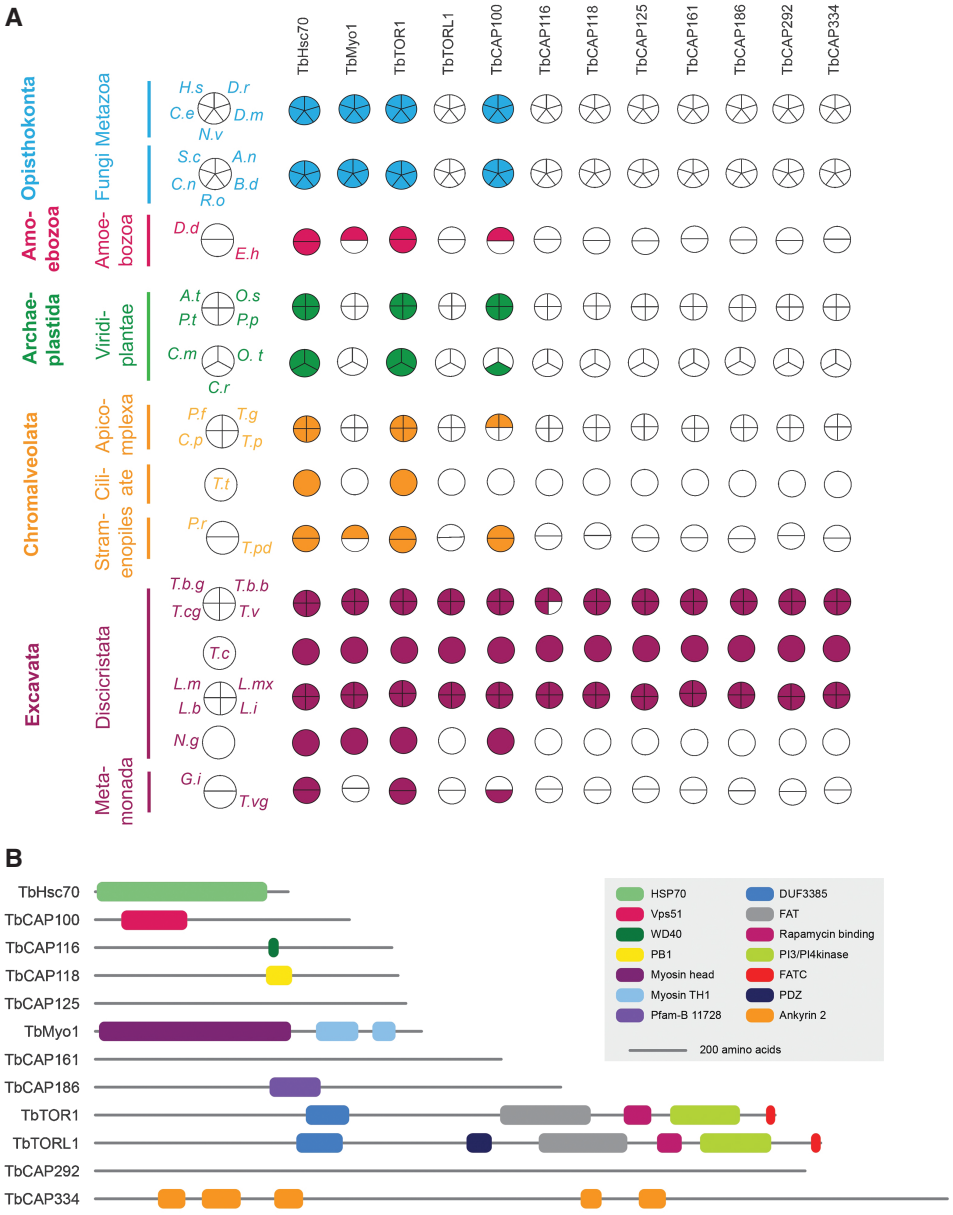

Figure 3: Evolutionary distribution and domain organization of TbCAPs. A) Searches of representative genomes were performed using the TbCAP protein sequence as query (see *Methods*), and results are shown as a Coulson plot (99). Taxonomic groups are color-coded, and filled sectors represent the identification of orthologs while open sections represent species in which an identification that met the criteria for orthology could not be made. Species key: T.b.b, *Trypanosoma brucei brucei*; T.b.g, *T. brucei gambiense*; T.c, *T. cruzi*; T.cg, *T. congolense*; T.v, *T. vivax*; L.m, *Leishmania major*; L.mx, *L. mexicana*; L.b, *L. brasiliensis*; L.i, *L. infantum*; N.g, *Naegleria gruberi*; G.i, *Giardia intestinalis*; T.vg, *Trichomonas vaginalis*; P.f, *Plasmodium falciparum*; T.g, *Toxoplasma gondii*; C.p, *Cryptosporidium parvum*; T.p, *Theileria parva*; T.t, *Tetrahymena thermophila*; P.r, *Phytophthora ramorum*; T.pd, *Thalassiosira pseudonana*; A.t, *Arabidopsis thaliana*; O.s, *Oryza sativa*; P.t, *Populus trichocarpa*; P.p, *Physcomitrella patens*; C.m, *Cyanidioschyzon merolae*; O.t, *Ostreococcus tauri*; C.r, *Chlamydomonas reinhardtii*; D.d, *Dictyostelium discoideum*; E.h, *Entamoeba histolytica*; H.s, *Homo sapiens*; D.r, *Danio rerio*; D.m, *Drosophila melanogaster*; N.v, *Nematostella vectensis*; C.e, *Caenorhabditis elegans*; S.c, *Saccharomyces cerevisiae*; A.n, *Aspergillus nidulans*; B.d, *Batrachochytrium dendrobatidis*; R.o, *Rhizopus oryzae*; C.n, *Cryptococcus neoformans*. B) TbCAP protein sequences were used to query protein domain databases (see *Methods*). Proteins are represented as a gray line with the N-terminus at left and are drawn to scale. Domain key: HSP70, 70 kDa heat shock proteins; Vps51, vacuolar protein sorting-associated protein 51/67; WD40, WD40 repeat; Myosin_head, myosin head (motor domain); Myosin_TH1, myosin tail; DUF3385, domain of unknown function; PDZ, post-synaptic density protein (PSD95); FAT, FRAP, ATM and TRRAP; Rapamycin_bind, Rapamycin binding domain; PI3_PI4_kinase, phosphoinositide 3-kinase; FATC, FRAP, ATM, TRRAP C-terminal; Ank_2, Ankyrin repeat.

PDZ in TbTORL1 (Figure 3). The PDZ is a protein interaction domain mostly present in multidomain proteins (64) and incorporating into complexes such as signaling complexes at the cell membrane (65,66). The other domains are the FAT (FRAP, ATM and TRRAP), rapamycin binding domain, phosphatidylinositol 3- and 4-kinase (PI3_PI4 kinase) and FATC (FAT domain at C-terminal) domains. This multidomain nature is in agreement with the proteins being members of TOR complexes and, by extension, possibly interacts with other protein complexes.

Eight TbCAPs were present only in *Trypanosoma* and *Leishmania*: TbCAP116, TbCAP118, TbCAP125, TbCAP 161, TbCAP186, TbCAP292, TbCAP334 and TbTOR-like 1. Domain searches were used to annotate this cohort (Figure 3). TbCAP116 and TbCAP118 have C-terminal WD40 and PBI domains respectively predominantly associated with protein complexes (67,68). TbCAP125, TbCAP161, TbCAP186 and TbCAP292 lack known domains. TbCAP334 has several ankyrin repeats, a scaffolding domain for protein-protein interactions as well as roles in protein trafficking; this extended structure suggests that TbCAP334 is involved in extensive interactions and potentially a structural/organizational role, and appears unique to trypanosomes (69,70). Other eukaryotic ankyrins of similar size, specifically ankyrin G, have a standard domain organization of an N-terminal membrane-binding domain composed of ankyrin repeats, a central spectrin-binding domain and a C-terminal regulatory domain of death and C-terminal domain (71,72).

Co-immunoprecipitation of proteins experimentally validated to interact, directly or indirectly, with clathrin (including TbHsc70, TbMyo1 and members of the TbTOR signaling pathway) indicates successful sampling of clathrin-interacting proteins. The identification of novel gene products with unknown domains, as well as domains implicated in protein complexes and trafficking, suggests a divergent clathrin interactome in *T. brucei*.

Developmental gene expression

In *T. brucei* many factors involved in trafficking are regulated at the transcript and/or protein level in a differentiation-dependent fashion (38,73); upregulation is frequently observed in the mammalian stage and is an indication of potential involvement in endocytic pathways. Relative mRNA expression levels were determined by quantitative reverse transcriptase-polymerase chain reaction (qRT-PCR). Five TbCAPs, TbHsc70, TbMyo1, TbCAP100 TbCAP116 and TbCAP118 were up-regulated in BSF (Table 2). Upregulation of TbMyo1 is consistent with Spitznagel et al. (26) where a threefold increase in the BSF was also observed. TbCAP161, TbCAP292 and TbCAP336 are expressed at equivalent levels in both life stages, while TbCAP125 and TbCAP186 are downregulated in BSF by twofold. TOR signaling proteins TOR1 and TORL1 are also downregulated by 5 and 10-fold, respectively in the BSF. While upregulation of the uncoating TbHsc70 and TbMyo1 was expected, the interaction and co-localization of TbCAP100, TbCAP116 and TbCAP118 with clathrin and upregulation in BSF supports a possible role in endocytosis.

Table 2: TbCAP developmental regulation and RNAi analysis following induction

Gene	qRT-PCR BSF/PCF	Residual RNA (%)	Proliferation index (control = 1.0)
TbHsc70	3.0	25 ± 4	0.04
TbMyo1	2.9	7 ± 1	0.20
TbTORL1	0.1	48 ± 4	0.03
TbCAP100	1.5	52 ± 17	0.11
TbCAP116	10.1	57 ± 9	0.09
TbCAP118	2.0	28 ± 1	0.10
TbCAP125	0.5	17 ± 2	0.10
TbCAP161	0.9	42 ± 4	0.17
TbCAP334	1.1	44 ± 12	0.20
TbCAP292 (24 h)	1.3	69 ± 5	1.00
TbCAP292 (72 h)	ND	27 ± 8	0.50

Developmental regulation of TbCAPs at the mRNA level was determined in triplicate by qRT-PCR as the ratio of mRNA levels in BSF to PCF. The residual mRNA levels after induction for 48 h (24 and 72 h for TbCAP292) was determined by qRT-PCR and the impact on growth expressed as a proliferation index based on determination of cell numbers over at least a 5 day period (see *Methods*).
ND, not determined.

TbCAPs are required for normal cell proliferation

The function of each candidate was investigated by gene silencing. In all cases, protein ablation triggered by RNA interference (RNAi) resulted in a significant defect in cell proliferation (Table 2). Loss of viability was observed within 48 h for all TbCAPs except TbCAP292, which required 72 h for a defect to fully manifest. The most severe impact was observed for TbTORL1 in which significant cell death occurred within 24 h. qRT-PCR demonstrated that the gene silencing was specific, with loss of over 30% of the target mRNA (Table 2). These data indicate that ten TbCAPs are highly important for cellular function in BSF.

TbCAPs are required for normal cell-cycle progression

We investigated the contributions of the TbCAPs on cell cycle progression by assessing the position of RNAi-induced cells in the cell cycle. In trypanosomes the temporal classification of individual cells to particular points in the cell cycle is eased by the consistent appearance of identifiable morphological changes to DNA-containing organelles at specific times. At the start of the cell cycle, trypanosomes have one kinetoplast (K) and one nucleus (N), referred to as 1K1N cells. The kinetoplast divides first resulting in 2K1N cells, which later go through mitosis (2K2N), and finally cytokinesis to create two daughter 1K1N cells. The frequency of cells with more than two kinetoplasts and nuclei (>2K2N) increased between 5 and 20-fold upon ablation of eight TbCAP RNAi mutants (Figure 4). TbCAPs do not play major roles in segregation of the nucleus and kinetoplast. Rather,

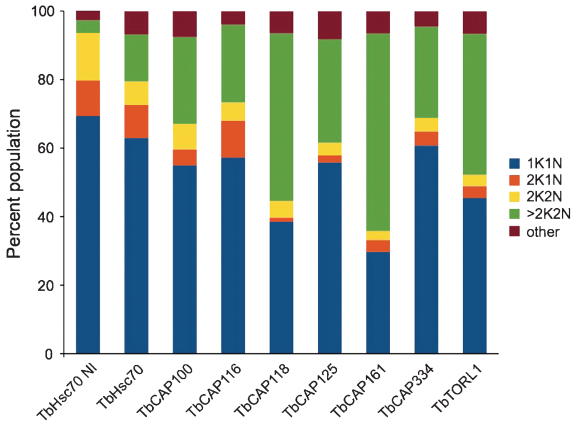

Figure 4: Knockdown of TbCAPs inhibits cell cycle progression. Select TbCAPs were analyzed for their importance in general cell cycle progression using specific RNAi-mediated knockdown (see *Methods*). After RNAi induction, both induced and non-induced RNAi cell lines were fixed and DAPI stained. Cells were scored for the number of kinetoplasts (K) and nuclei (N). $n = >200$ cells for each TbCAP. TbHsc70 NI correspond to the non-induced (NI) state of this cell line, and is representative of all other TbCAP KDs analyzed here but not shown. TbCAP KD induced cells are designated at bottom.

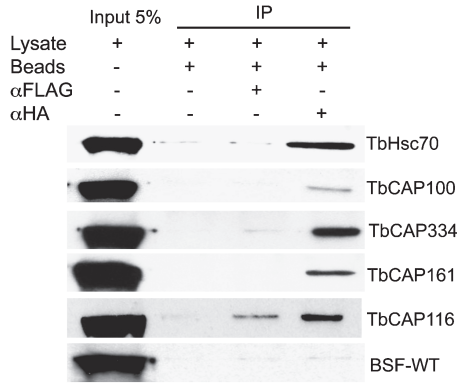

Figure 5: Reverse co-immunoprecipitation validates clathrin interaction. Immunoprecipitation of HA fused versions of a selection of TbCAPs was performed and following resolution by SDS-PAGE the isolated complexes were probed for anti-TbCHC western blot. αFlag: monoclonal anti-Flag antibody and αHA: monoclonal anti-HA antibody. TbCAPs are designated at right.

higher levels of cells with >2K2N suggests that cells successfully reach the G_2/M phase, but fail cytokinesis and progress into a next G_1 stage. A defect in cytokinesis is a frequent phenotype associated with disruption of membrane trafficking and targeting.

Reverse co-immunoprecipitation

Co-localization together with immunoisolation provides strong evidence that the TbCAPs represent direct or indirect clathrin interacting proteins. To further validate the TbCAPs as genuine clathrin interaction partners, immunoprecipitations using monoclonal antibody anti-HA on selected HA-tagged TbCAPs over-expressed in trypanosomes were fractionated by SDS-PAGE, transferred to membranes and probed with anti-TbCHC antibody. Immunoprecipitations of TbHsc70, TbCAP100, TbCAP116, TbCAP161 and TbCAP334 carried out in this manner successfully co-precipitated clathrin, providing further validation of these TbCAPs as *bona fide* clathrin-interacting proteins and suggesting that most of the remaining TbCAPs are also likely to be genuine clathrin-interacting proteins (Figure 5). Similar IPs performed using anti-FLAG antibodies did not precipitate equivalent levels of clathrin, nor did anti-HA pullouts of wild-type cells, suggesting that the retrieval of clathrin depends on the presence of the HA-tagged TbCAP. Note that clathrin is both a high abundance protein that participates in many interactions, and hence the comparatively low yields of clathrin in the HA-IPs are not unexpected.

TbCAPs are involved in internalization of GPI-anchored cell surface proteins

To investigate the roles of TbHsc70, TbCAP100, TbCAP116, TbCAP161 and TbCAP334 in endocytosis, internalization of fluorescein-conjugated concanavalin A (FITC-ConA) following RNAi induction was monitored. ConA principally binds mannose-containing VSG molecules (74) and is subsequently routed from the FP to the lysosome, making it a suitable marker for membrane-bound endocytic activity (75). In RNAi-induced cell lines, a significant reduction in intracellular pools of FITC-ConA was observed (Figure 6), an indication of defective uptake of VSG. The extent of the defect was quantitated by single cell immunofluorescence examination of the intracellular pool; internalized FITC-ConA in RNAi-induced cells were low at early time points post-induction (data not shown) for TbCAP100, TbCAP116, TbCAP161 and TbCAP334. For TbHsc70, the internal ConA pool was almost unaltered at early time points, but in all cases reduced trafficking deeper into the cells and into the terminal endosomal compartments was observed. This is at variance from RNAi against clathrin, where ConA accumulation at the FP is observed (16).

Further investigations of ConA uptake in cells sorted based on their DNA content and analyzed by FACS confirmed the defective internalization upon ablation of TbCAPs. The phenomenon is neither cell cycle-dependent, nor a result of a disruption in cell cycle progression (Figure 6C). Together, these data suggest that TbHsc70, TbCAP100, TbCAP116, TbCAP161 and TbCAP334 are involved in VSG trafficking in BSF trypanosomes.

TbCAPs are involved in trafficking of cell surface trans-membrane domain proteins

To further investigate silencing effects on endocytosis, we assessed the impact on the most abundant surface *trans*-membrane protein, the invariant surface glycoprotein ISG75 (30,27). A significant decrease in intracellular pools of ISG75 was observed by immunofluorescence on ablation of TbHsc70, TbCAP100, TbCAP116 and

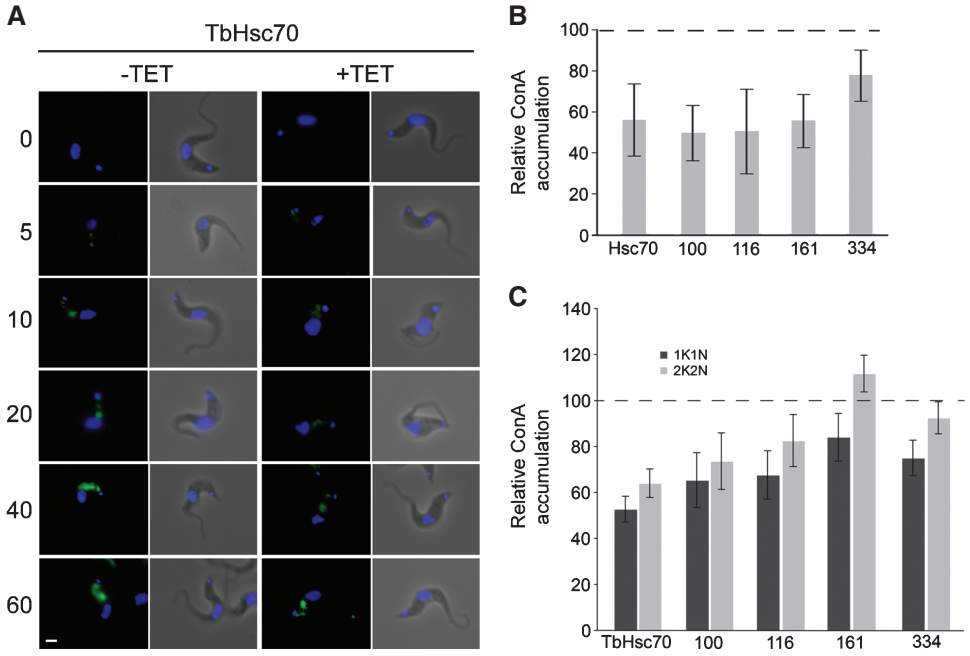

Figure 6: Several TbCAPs participate in endocytosis. A) Representative VSG internalization in presence and absence of TbHsc70 knockdown. After 36 h, induced and non-induced RNAi cell lines were incubated with FITC-ConA at 37°C and aliquots prepared for immunofluorescence. The intracellular pool is clearly reduced in RNAi-induced cells. B) Single cell quantitation of intracellular conA pool after 20 min uptake in selected TbCAP RNAi lines. $n = >20$ cells for each analysis. Error bars are the standard deviations. C) Flow cytometric analysis of FITC-ConA uptake after 20 min. Aliquots of cells were incubated with Hoechst to stain DNA and analyzed by FACS. The level of the intracellular FITC-ConA pool was determined separately for cells at interphase (1K1N) and post-mitotic (2K2N) to reduce the influence of cell size on FITC-ConA label intensity. At least 10 000 cells were analyzed for each determination. The experiment has been performed twice with essentially identical results; error bars indicate the standard error. Scale bar (lower left) = 1 μM.

TbCAP161 (Figure 7A and C). Conversely, ablation of TbCAP334 resulted in increases to the intracellular ISG75 pool. To ensure that these effects are not due to altered ISG75 expression, whole cell lysates were subjected to Western blot analysis using polyclonal antibody anti-ISG75 (Figure 7B). ISG75 levels were essentially unaltered, indicating that the changes to internal pools result from trafficking defects rather than steady state abundance, although we were unable to detect a significant increase in the surface abundance of ISGs based on antibody staining of non-permeabilized cells (data not shown). In agreement with ConA uptake, these data suggest a role for TbHsc70, TbCAP100, TbCAP116 and TbCAP161 in endocytosis, with an ISG75 trafficking defect similar to ablation of clathrin (27) and TbEpsinR (30). Conversely, the increase in intracellular ISG75 resulting from TbCAP334 ablation suggests an involvement in later events that potentially alter turnover or recycling of ISG75. This could be consistent with conserved roles for ankyrin in late endosome, lysosome (76,77) and Golgi apparatus trafficking (78,79). While the increase in internal ISG75 in TbCAP334 knockdown cells and apparent block to uptake for the remaining TbCAPs and TbHSC70 may seem at variance with the lack of an alteration to steady state mechanisms, previous work has suggested the presence of a compensatory mechanism to maintain overall copy number, which may also operate here (27). Further, due to the saturating levels of VSG at the cell surface, monitoring of ISG levels is somewhat inaccurate, and while an inability to detect increased surface ISG is likely due to this, we cannot rule out other trafficking defects. In conclusion, these data indicate the involvement of the TbCAPs and TbHsc70 in trafficking of ISG75.

To determine if impairment in bulk endocytosis and ISG75 internalization was associated with mis-localization and/or alterations in protein levels or endocytic compartments, immunofluorescence and western blotting were carried out for clathrin, TbEpsinR, TbRab11, p67 and TbRab5 (Figure S4). With the exception of a small decrease in TbRab5 in TbCAP161 knockdown cells at two days post-RNAi induction, no significant alterations were observed for any of these endocytic markers, suggesting that the TbCAP knockdowns did not significantly affect the morphology of early endosomes, recycling endosomes or the lysosome (Figure S4A). In addition, there was no change in abundance of these marker proteins (Figure S4B), distinct from the dramatic effects obtained by TbRab5A knockdown where coordinate loss of TbCHC is also observed (63). Moreover, in TbCAP161 the moderate effect following ablation of TbRab5A was not propagated through to changes in TbCHC levels, and these data suggest that the endocytic effects of knockdown of TbHsc70, TbCAP100, TbCAP116, TbCAP161 and

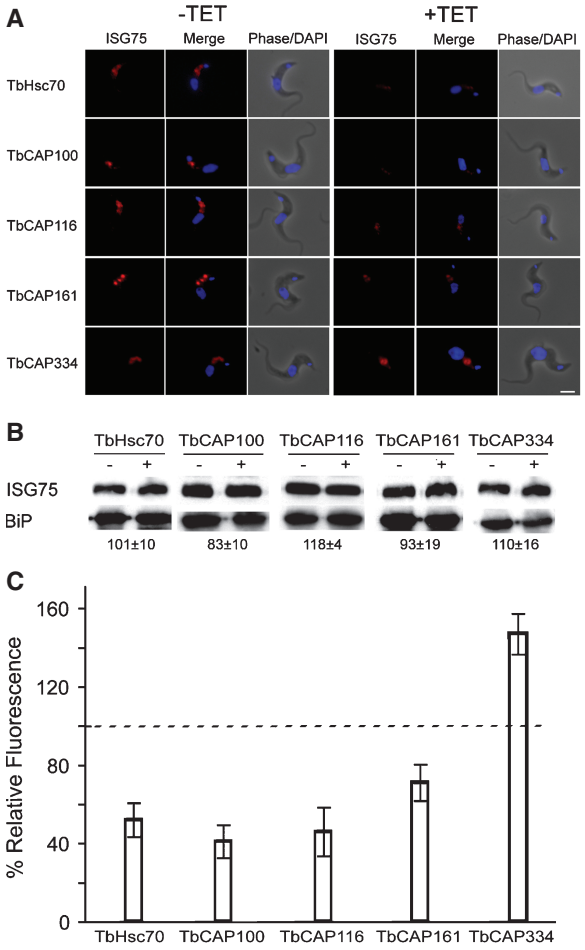

Figure 7: Several TbCAPs are involved in the internalization of ISG75. A) Immunofluorescence analysis of ISG75 following knockdown of TbCAPs. After RNAi induction, cells were prepared for immunofluorescence and stained for the major surface/endosomal transmembrane protein ISG75 (red) and DNA (blue). The intracellular ISG75 pool was significantly reduced on depletion of TbHsc70, TbCAP100, TbCAP116 and TbCAP161, while an increase was observed for TbCAP334. Scale bar = 2 μM. B) western blot analysis of whole cell lysates for ISG75, with TbBiP used as a loading control. ''−'' and ''+'' indicate uninduced and induced cells respectively. Numbers below the panels indicate quantitation using underexposed films; data are the mean ± SD from three experiments. C). The percent relative intracellular ISG75 quantified by single cell fluorescence analysis as shown in (A). Bars are data for induced cells ($n => 20$ cells) for each determination and error bars indicate the standard deviation of the data. Dotted line indicates 100% for non-induced cells to which the induced data have been normalized.

TbCAP334 are specific and not due to secondary defects.

Knockdown of TbCAPs cause defects in endocytosis dynamics and flagellar pocket morphology

To gain more insight into the roles TbCAPs play in endocytosis and how they may mediate the machinery, we studied RNAi mutants at ∼30 h pre- and post-induction by fast-isothermal fixation and transmission electron microscopy. In BSF, endocytosis and exocytosis occur at very high rates (24), and this high membrane turnover may explain the small volume of the FP in this life stage (particularly when compared to the FP of the insect form procyclic, where endocytosis is downregulated (38,40). The BSF FP is invariably associated with CCPs, CCVs and VSG-containing exocytic vesicles, and is in close association with the Golgi stack (81). Flat clathrin-coated lattices (CCLs) have been reported on the BSF FP membrane, and suggested to represent a reservoir of pre-assembled clathrin triskelions, poised to facilitate the high flux of endocytosis seen in these cells (81).

The presence of the RNAi construct did not change overall morphology of the FP as non-induced RNAi cell lines resembled the wild type (WT) BSF (see Figure 8, 'non-induced'). After RNAi induction however, thin-sections reveal an enlarged FP in TbCAP100, TbCAP116, TbCAP161 and TbCAP334 knockdowns (Figures 8 and 9C). An expanded FP suggests an endocytic block similar to those observed on knockdown of clathrin (16), TbRab5 (20), TbRab 11 (22) and TbARF1 (23), and is consistent with defects to internalization of surface proteins (Figures 6 and 7). By contrast, inactivation of TbHsc70 by RNAi did not phenocopy the TbCAP knockdowns, suggesting that TbHsc70 may play a role in clathrin biology elsewhere in the cell, or that the effects of this specific RNAi could not be detected or preserved by electron microscopy. Notably, other organelles involved in endocytosis and exocytosis (the Golgi, endosomes, lysosome and multivesicular bodies), appeared normal in TbCAP mutants (for a representative image see Figure 8, TbCAP100).

Alongside the severe effect in FP morphology, TbCAP100, TbCAP116, TbCAP161 and TbCAP334 knockdowns also presented multiple nuclei and flagella. This demonstrates that these cells were progressing through the cell cycle (initiating new rounds of S-phase and mitosis) but ceased dividing altogether and, as such, became monstrous, largely contorted cells (Figure 8, cf. Figure 4), and as noted above.

Close examination of TbCAP100, TbCAP116, TbCAP161 and TbCAP334 knockdowns revealed the presence of clathrin structures remaining associated with the enlarged FP membranes, either as deeply curved pits (of ∼100nm diameter, Figure 9A) or as flatter lattices (Figure 9B). The number of clathrin assemblies was quantified by morphometry. While there was no significant reduction in the total number of CCPs formed (Figure 9D), this equates to a substantial reduction in CCP density due to the large increase in flagellar pocket size (Figure 9C). There was also a significant increase in the formation of large CCLs (up to 1 μm long) in all four RNAi cell lines analyzed (Figure 9E). Assuming that CCPs can be formed from these lattices in trypanosomes in a manner similar to that seen in mammalian cells (82,83), it appears that,

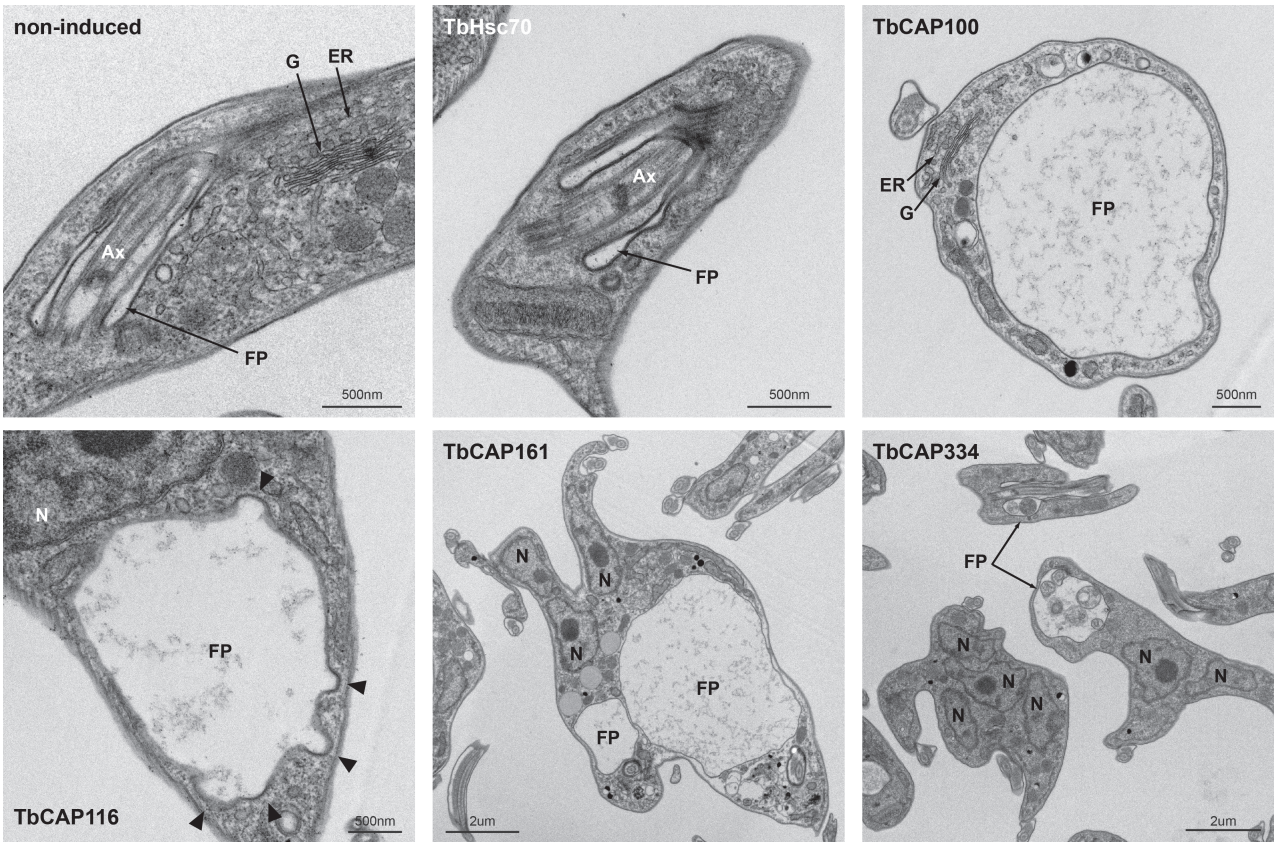

Figure 8: Ablation of TbCAPs leads to morphological defects and an enlarged flagellar pocket. Panels show thin-section transmission electron micrographs demonstrating the effect of protein ablation on cells from cultures at 30 h post RNAi induction. Knockdown of TbCAP100, TbCAP116, TbCAP161 and TbCAP334 results in enlargement of flagellar pockets and failure in cytokinesis (as illustrated by multiple nuclei and flagella). However, no gross morphological defect was seen in cells where TbHsc70 is ablated. Ax, axoneme; G, Golgi apparatus; ER, endoplasmic reticulum; N, nucleus. Arrowheads point at CCPs seen on the FP membrane. 'Non-induced' refers to TbCAP116 RNAi cells as a representative of the overall morphology prior to RNAi induction in all other cell lines.

in the absence of TbCAP100, TbCAP161 and TbCAP334, lattices fail to be curved into pits, and then to progress to form CCVs. Therefore, our observations suggest a role in promoting membrane curvature for these three CAPs. In fact, if these cells can recruit clathrin to their FPs, as is apparent, but the process of CCP formation is drastically slowed or completely blocked, a likely consequence is an expansion in FP volume, which may enable further recruitment of clathrin to the membrane and compromised endocytic activity.

In TbCAP116 knockdown cells the number of CCPs remained unaltered, or not significantly different from, non-induced cells (Figure 9D). However, here there was also an increase in the number of CCLs at the FP membrane (Figure 9E), and a more modest, twofold increase in overall FP size (Figure 9C). These results demonstrate that the knockdown cells are competent for membrane bending and CCP formation in the absence of TbCAP116, but there seems to be a delay in curving lattices into invaginations, which leads to accumulation of CCLs. Thus, the TbCAP116 knockdown phenotype appears to be an intermediate between the blocked endocytosis seen in TbCAP100, TbCAP161 and TbCAP334 knockdown cells and the fast endocytosis of non-induced or WT cells. We suggest that, in the less severe phenotype of TbCAP116, the additional FP membrane and the extra assembly of flat clathrin sheets have reached a balance, making the overall ratio of clathrin-coated/clathrin-uncoated FP membrane unchanged (Figure 9F). Perhaps unsurprising, this is in agreement with the less severe cytokinesis defect seen for TbCAP116 RNAi cells following induction (Figure 4).

Discussion

Understanding the evolutionary origins, diversity and functions of intracellular trafficking pathways across eukaryotes has benefited from extensive genome sequencing coupled to structural studies; these revealed unexpected connections between pathways, together with great complexity in the earliest eukaryotes, including those predating the LECA (84–87). This, together with recognition that

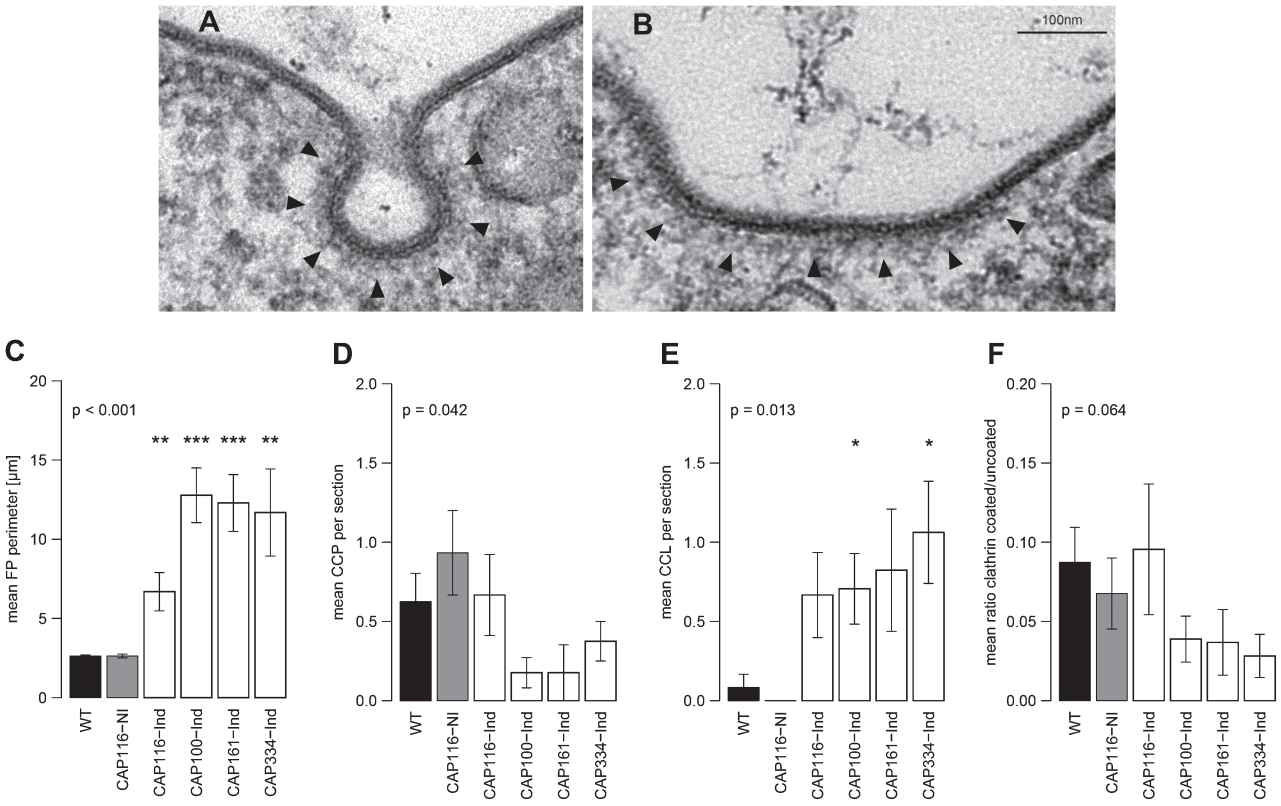

Figure 9: Ablation of TbCAPs does not prevent clathrin assembly, but affects vesicle formation. Clathrin was seen associated to the FP membrane of mutant cells as deeply curved coated pit (A) or large, flat coated sheets (B). Black arrowheads indicate clathrin assembly. C–F) Bar graphs display morphometric analysis done on electron micrographs ($n > 25$ FP profiles for each cell line). Bars represent standard error. Two-tail *t*-test with Bonferroni correction was used to assess for significant difference from WT cells; asterisks represent p-values smaller or equal to 0.01 (*), 0.002 (**) or 0.0002 (***). Overall p-value from an ANOVA test is provided on top left of each respective graphs. TbCAP116 non-induced cells were included in this analysis to show that any effect seen is not due to the presence of an RNAi construct, but to the induction of that specific RNAi; the same results were seen for all other non-induced TbCAP RNAi cells (data not shown).

many critical players mediating trafficking are members of paralogous families, i.e. coatomer, Rabs, SNAREs, etc., provides a simple but powerful paradigm for the evolution of new pathways. Secondary loss is also common, with the result that a better understanding of the drivers sculpting the endomembrane system is emerging, despite the absence of insights into how selective pressure has been applied (87). These *in silico* analyses, however, cannot capture much mechanistic detail, and more critically, due to the superior datasets available for animals and fungi, our view is subject to sampling bias.

One very ancient pathway is CME, but multiple modes of endocytosis are now recognized, defined by differential morphology and specific protein requirements (88). We asked if CME is mechanistically equivalent or distinct in diverse evolutionary lineages, especially as morphological data are unavailable or non-discriminatory for many organisms. We selected proteomics for unbiased sampling of clathrin-interacting proteins in *T. brucei*, an organism with considerable prior characterization of trafficking (3). CME is the sole endocytic mechanism in trypanosomes, but clathrin is also present on the Golgi complex and additional endosomal structures, suggesting involvement in multiple pathways, but with many conspicuous absences by *in silico* analysis; this includes for example orthologs of well characterized clathrin interactors like auxilin (35,16,10,29); Grunfelder et al., 2003). Subcellular fractionation in mammalian cells indicates substoichiometric relationships between clathrin and other CCV polypeptides (39), suggesting we would encounter low levels of clathrin associating proteins. Consequently we designed a hierarchical validation strategy (Figure S1), incorporating localization, reverse immunoisolation and gene silencing for direct functional inference of *bona fide* clathrin association.

We identified a large cohort of proteins, many of which are likely clathrin-associated, and selected the most significant for initial validation by localization, and validated twelve proteins with high confidence as TbCAPs, including several expected proteins, i.e. TbHsc70, TbMyo1 and TbTOR2, based on known functions in other organisms (TbHsc70) or trypanosomes

(TbMyoI and TbTOR2; (42,26)). The location reported here for TbTOR1 and TbTORL1 is at variance with that reported recently using polyclonal antibodies (42,43), and therefore the direct association of these molecules with clathrin-containing endomembrane compartments is uncertain. Of the remaining proteins, only TbCAP100, had broad taxonomic representation, and the remainder appeared restricted to trypanosomatids. Surprisingly, this distribution excluded metamonads, a sub-branch of the Excavata, suggesting restricted distribution, which may reflect trypanosomatid-specific mechanisms subtending clathrin trafficking pathways. Interestingly, TbCAP100 bears a Vps51/67 domain, and is likely the ortholog of *H. sapiens* Vps51.

Of the trypanosome-specific cohort, four have no assignable domains while the remainder lack an obvious functional signature. The presence of WD40 and ankyrin domains in TbCAP116 and TbCAP334 suggests roles in protein–protein interactions, and evidence from gene silencing does indicate specific functions in endocytosis. The frequent emergence of a cytokinesis failure phenotype is one that is associated with many trafficking blocks and likely reflects incorrectly targeted protein and/or lipids to the cytokinesis furrow or other replicating structures at cell division. A specific impact on ConA internalization was also found on silencing of TbHsc70, TbCAP100, TbCAP116, TbCAP161 and TbCAP334, suggestive of a failure to endocytose VSG. This conclusion is supported by a decreased intracellular pool of ISG75 in Tb Hsc70, TbCAP100, TbCAP116 and TbCAP161 KD cells, which indicates defects in early stages of endocytosis. Whereas increased internal levels of ISG75 for TbCAP334 suggest functions later in the endosomal system, allowing internal accumulation but decreased turnover of ISG75, by either defects in recycling or late endocytic steps (27,41). The presence of a BigEye phenotype is both consistent with a role in CME, but also suggests a less prominent role than clathrin itself, and is more reminiscent of the phenotype of TbEpsinR silenced cells (30).

Our electron microscopy analysis revealed finer details of the effect of protein ablation, and allowed us to start to assign TbCAPs into different molecular functions: TbCAP100, TbCAP161 and TbCAP334 seems to be required for the curving of flat areas of clathrin-coated FP membrane to give rise to CCPs. Indeed, in the absence of these proteins, the FP can still recruit and assemble clathrin, but CME is blocked by prevention of CCP formation. TbCAP116 seem to play a different role: upon ablation of the protein, cells are competent for CCP formation, although the process is somehow delayed. Importantly, all of these data support roles for TbCAP100, TbCAP116, TbCAP161 and TbCAP334 at post-recruitment steps, consistent with the isolation protocol used, which included detergent, and hence indicating that these TbCAPs likely function in the removal of clathrin from the membrane. Interestingly, many of the proteins known to be involved in CCP neck constriction and scission are unidentified in the trypanosome genome (89), suggesting that TbCAPs represent a mechanism that arose specifically in the trypanosome lineage. Ongoing investigations are directed at exploring clathrin membrane anchors and interactions with the actin system.

A unifying aspect of ablation of different TbCAPs is that the absolute amount of clathrin triskelion being recruited to the FP is increased, and much of this additional clathrin is assembled into large flat sheets that fail or delay to mature into pits. Clathrin, as well as F-Bar and ENTH-domain containing proteins have been implicated as initiators of membrane curvature. Our genetic analysis coupled with ultra-structural studies suggests that TbCAPs function in the same pathway, although their precise mechanistic action remains to be elucidated. The presence of large expansions of flat clathrin-coated membrane is distinct from a model of gradual addition of triskelions to a growing, highly curved invagination (90), and favors a mechanism of pre-assembly of flat lattices as clathrin reservoirs to sustain the formation of a large number of coated pits and vesicles (91,92). This may reflect a specific adaptation to support the extremely fast endocytic flux at the FP.

Why does ablation of TbCAPs cause a severe cytokinesis defect? It is relevant here to recognize that TbCAPs may participate in functions beyond CME. A cytokinesis failure is unlikely to be a result of starvation as RNAi-induced cells are growing in size, divide internal organelles and complete mitosis. The defect is specific to cell division, and raises the possibility that TbCAPs function in signaling, recruiting division machinery components, and/or assembly of the cleavage furrow. Alternatively, the cytokinesis failure could be a secondary effect resulting from morphological defects. Specifically, an enlarged FP may perturb the highly ordered spatial polarization of the cell and impair the precise positioning and migration necessary for cell division. Similar effects have been observed by RNAi-mediated ablation, in this particular life cycle stage, of proteins involved in flagellar motility (93), and as well as for silencing of other endocytic components.

Overall, while the precise functions of most TbCAPs remain to be fully elucidated, our data indicate that a highly divergent clathrin interactome in trypansomes and consistent with earlier *in silico* predictions. However, the system is not necessarily simplified, but rather may comprise a cohort of *pan*-eukaryotic proteins together with a lineage-specific group, precisely as the animal and fungal systems. This suggests that CME and other clathrin-mediated functions are mechanistically divergent, and the simple designation of pathways as clathrin-dependent or independent fails to capture the true functional diversity between lineages. Of interest here is that several of the conserved interaction sites in the N-terminal region of the clathrin heavy chain remain well conserved between trypanosomes and higher eukaryotes including clathrin

box motif (CBM) (*H. sapiens* TLQIF/KMK, *T. brucei* NLQIF/RLK) and the recently described fourth site (*H. sapiens* EHLQLQN versus *T. brucei* EVFGLNS) (94). By contrast the AP-2 binding site does not appear retained (*H. sapiens* 188-RKVSQ versus *T. brucei* NNSGR), fully consistent with the loss of AP-2.

The uncovering of the TbCAPs also provides potential for detailed mechanistic analysis of CME in trypanosomes. This mechanistic diversity has several parallels: e.g. (i) the independent evolution of ARF proteins between *Trypanosoma* and Opistokhonta (95), where the functions of these small GTPases are likely highly novel; and (ii) perhaps more similarly, the unique compartmentalization of glycolysis by *Trypanosoma* into the glycosome, such that an otherwise conventional pathway is sequestered and controlled by highly distinct mechanisms compared with mammalian cells, and which offers therapeutic potential (96). We suggest that the mechanistic details of trypanosome CME may also offer such opportunity due to high levels of diversity between the parasite and host.

Materials and Methods

Cell lines

Trypanosoma brucei BSF and PCF Lister 427 laboratory-adapted strains were routinely cultured in HMI9 and SDM79 media, respectively, supplemented with 10% fetal calf serum. For RNAi analysis, the single marker T7 RNAP/TETR BSF cells (SMB; (97)) were used. SMB cells were continuously maintained in the presence of 2.5 μg/mL G418 and in G418 plus hygromycin (Sigma; 2.5 μg/mL) for cells transfected with p2T7 RNAi plasmid constructs. The density of RNAi cell lines was maintained between 1×10^5 and 2×10^6 cells/mL and induction carried out in the presence of tetracycline (Sigma) at 1.0 μg/mL. Cell concentration was determined using a coulter counter (Beckman). Transgenic BSF-427 lines expressing HA-tagged chimeric protein were continuously cultured in the presence of 2.5 μg/mL neomycin (Sigma).

Immunoprecipitation

A total of 2×10^8 cells were harvested by centrifugation and washed twice with PBS. Cells were resuspended in 200 μL of RIPA buffer [25 mM Tris–Cl pH 7.5, 150 mM NaCl, 1% NP-40, 0.5% sodium deoxycholate, 0.1% SDS, plus protease inhibitor cocktail (Roche)] and incubated on ice for 15 min with brief mixing. Thereafter, the lysate was centrifuged at 20 000 × ***g*** for 10 min at 4°C and the supernatant transferred to a new microcentrifuge tube and an equal volume of dilution buffer (1.25% Triton X-100, 190 mM NaCl, 50 mM Tris pH 7.5, 6 mM ethylenediaminetetraacetic acid, protease inhibitor cocktail) added. To immunoprecipitate putative clathrin – TbCAP complexes, the lysate was incubated for 1.5 h at 4°C with 3 μL of rabbit TbCHC antibody (35) and complexes subsequently bound to 20 μL of protein A Sepharose beads (Sigma) under the same conditions. Non-immune rabbit serum and protein A beads alone were used as controls accordingly. The beads were washed multiple times with ice-cold PBS, resuspended in Laemmli buffer and heated at 95°C for 5 min. The isolates were separated by SDS-PAGE and silver stained or western blotted. For reverse co-immunoprecipitation of HA-tagged cell lines, ~10^9 cells were lysed in 600 μL RIPA buffer and lysates prepared as above. The total lysate was divided into three equal parts and each incubated with mouse anti-HA (1:100; Invitrogen), mouse anti-Flag (1:100; Sigma, negative control) or a no antibody negative control. Co-immunoprecipitation from BSF lysates was also performed under identical conditions.

Identification of proteins by MS

For MS identification of clathrin-associated protein (TbCAP) candidates, in-gel digestion of resolved lysates was performed. Coomassie stained gel bands were excised and transferred into a 96-well PCR plate. All subsequent sample preparation was performed using a Mass Prep Station (Micromass). Briefly, gel bands were destained, reduced (dithiothreitol), alkylated (iodoacetamide) and subjected to enzymatic digestion with trypsin overnight at 37°C. After digestion, 10 μL of the supernatant was pipetted into a sample vial and loaded onto an autosampler for automated LC-MS/MS analysis. Three fully independent co-immunoprecipitations and MS analyses were carried out.

All LC-MS/MS experiments were performed using an Eksigent NanoLC-1D Plus (Eksigent Technologies) HPLC system and an linear trap quadropole (LTQ) Orbitrap mass spectrometer (ThermoFisher). Separation of peptides was performed by reverse-phase chromatography using a flow rate of 300 nL/min and an LC-Packings (Dionex) PepMap 100 column (C18, 75 μM i.d. × 150 mm, 3 μM particle size). Peptides were loaded onto a precolumn (Dionex Acclaim PepMap 100 C18, 5 μM particle size, 100A, 300 μM i.d × 5 mm) from the autosampler with 0.1% formic acid for 5 min at a flow rate of 10 μL/min. After this period, the valve was switched to allow elution of peptides from the precolumn onto the analytical column. Solvent A was water + 0.1% formic acid and solvent B was acetonitrile + 0.1% formic acid. The gradient employed was 5–50% B in 40 min. The LC eluant was sprayed into the mass spectrometer by means of a New Objective nanospray source. All *m/z* values of eluting ions were measured in the Orbitrap mass analyzer, set at a resolution of 7500. Peptide ions with charge states of 2+ and 3+ were then isolated and fragmented in the LTQ linear ion trap by collision-induced dissociation and MS/MS spectra were acquired. Post-run, the data were processed using Bioworks Browser (version 3.3.1 SP1, ThermoFisher). Briefly, all MS/MS data were converted to dta (text) files using the Sequest Batch Search tool (within Bioworks). The dta files were converted to a single mgf file using an SSH script in the SSH Secure Shell Client program (Version 3.2.9 Build 283, SSH Communications Corp.). These combined files were then submitted to the Mascot search algorithm (Matrix Science) and searched against a *T. brucei* predicted proteome database, using a fixed modification of carbamidomethyl and variable modifications of oxidation (M).

Informatics

Annotations for the predicted proteins identified by MSMS were retrieved from www.genedb.org. Due to the large size of the dataset, criteria for selection of candidates for further investigation was set to include recovery in two or three of the analyses, the presence of protein domains involved in trafficking or protein-protein interactions and/or known involvement in trafficking were used; these criteria likely lead to under-representation of novel gene products and favor high abundance proteins. Occurrence in multiple MS was accorded a higher score. Proteins that failed to match all of these criteria were rejected from further analysis. To investigate the phylogenetic distribution of selected candidates across the eukaryotic lineage, BLAST searches were carried out against selected proteome databases, chosen for completeness and taxonomic coverage. The kinetoplastids *Trypanosoma congolense*, *T. vivax*, *T. brucei gambiense*, *T. cruzi*, *L. major*, *L. braziliensis*, *L. mexicana*, *L. infantum* and *Crithidia fasciculata* were at geneDB (www.geneDB.org) and TriTrypDB (http://tritrypdb.org/tritrypdb/). *Naegleria gruberi* (*N. gruberi*) was at the Joint Genome Initiative (http://genome.jgi-psf.org), *Trichomonas vaginalis* (*T. vaginalis*) at http://trichdb.org/trichdb/, *Giardia intestinalis* (*G. intestinalis*) at http://giardiadb.org/giardiadb/, *Toxoplasma gondii* (*T. gondii*) at http://toxo.org/toxo/, *Arabidopsis thaliana* (*A. thaliana*) at www.arabidopsis.org and www.plantgdb.org/AtGDB, *Saccharomyces cerevisiae* (*S. cerevisiae*) at http://www.yeastgenome.org/ and http://mips.helmholtz-muenchen.de/genre/proj/yeast/ and *Plasmodium falciparum* at http://plasmodb.org/plasmo/. Searches were also carried out at National Center for Biotechnology Information (NCBI) (blast.ncbi.nlm.nih.gov/Blast.cgi). A similar search was carried out on an internally available protein database of sequenced eukaryotic supergroups

(98), and a harmonized final data set from these three approaches used to generate a Coulson plot of ortholog distribution Field, Coulson and Field, unpublished. Protein domain searches were carried out at Pfam [http://pfam.sanger.ac.uk/search; (99)], InterPro (http://www.ebi.ac.uk/Tools/InterProScan/; (100)) or PROSITE (http://www.expasy.ch/prosite/; (101)).

Plasmid constructions and transfections

Protein candidates encoded by gene products less than 3 kb in size were amplified and cloned into pXS5 (18) vectors, forming constructs for ectopic expression of C-terminal HA-, FLAG- or GFP-tagged proteins. For RNAi, silencing fragments were determined using RNAit (102) and constructs prepared in the p2T7 vector system (103). About 15 μg of vector was linearized with either XhoI or BsmI (NEB) for pXS5 tagging and NotI (NEB) for p2T7-RNAi constructs. For chromosomal HA- or GFP-tagging (genes above 3 kb), the method of Oberholzer et al. (104) was applied. The manipulated or amplified regions of all constructs were sequenced prior to use by dye-deoxy sequencing for validation. Transgenic BSF lines were generated by electroporation using an Amaxa Nucleofector® II, incubation for 6–8 h and selection in presence of the appropriate drug. Viable cells taken from plates where less than 50% of wells contained transformants were considered clonal and further expanded in continuous presence of antibiotic(s).

RNA interference

Induction of RNAi was carried out in the presence of tetracycline (1 μg/mL) on mid-log phase cells. Proliferative rates were monitored as above for induced and non-induced cells maintained at densities between 1×10^5 and 2×10^6/mL. Aliquots of cells were used for determination of ablation of the targeted open reading frame by qRT-PCR and western blot.

Western blotting

After resolution of protein lysates by 12.5% SDS-PAGE, the proteins were transferred onto polyvinylidene fluoride (PVDF) membranes (Millipore). Non-specific sites on the membrane were blocked, and western blot was carried out following standard procedures. Rabbit polyclonal antibody against TbCHC (35), TbEpsinR (30), TbRab11 (105), TbRab5 (18) and TbBiP (106) and monoclonal anti-HA (Roche) were used at concentrations previously described (30,27). Horseradish peroxidase conjugated rabbit anti-mouse and goat anti-rabbit (Sigma) secondary antibodies were used at 0.2 μg/mL concentration. Detection by enhanced chemiluminescence and exposure to X-ray film were used to detect bound antibodies.

Endocytosis assays

Log phase RNAi cell lines were diluted into two aliquots (10^5 cells/mL) and RNAi induced by addition of tetracycline (1 μg/mL) for 48 h. Control cells were non-induced. The cells were harvested, washed once with serum free HMI-9 supplemented with 1% BSA and re-suspended at ~10^7/mL. The cells were starved for 30 min prior to addition of Concanavalin A Alexa Fluor 633 conjugate (ConA) (5 μg/mL; Molecular Microbes). Every 10 min 1 mL aliquots were removed and added to 9 mL of ice-cold Voorheis's-modified phosphate-buffered (vPBS) to inhibit further uptake. The cells were prepared for immunofluorescence and images captured as below for wide field microscopy under the same exposure conditions. Fluorescence levels in individual cells were determined using METAMORPH software (Universal Imaging Corp.).

For FACS, ConA Alexa Fluor 633 conjugate (5 μg/ml; Molecular Microbes) was used. A total of 2×10^6 cells were recovered after appropriate time points as above and added to 9 mL ice-cold PBS. The cells were washed twice with PBS and resuspended in 1% formaldehyde in PBS. To stain DNA, the cells were incubated with Hoechst (Molecular Microbes) at 37°C for 10 min. Fluorescence from 50 000 cells with 2n DNA content (i.e. interphase) was measured using Cyan ADP (DakoCytomation). Data were analyzed with SUMMIT Software (Cytomation).

Immunofluorescence microscopy

Mid-log phase cells were harvested and washed with ice-cold vPBS. The cells were subsequently fixed in 4% paraformaldehyde and adhered to poly-lysine coated slides (VWR). For permeabilization and staining of internal structures, the cells were incubated with 0.1% Triton X-100 in PBS, washed with PBS and blocked with 20% fetal bovine serum in PBS. For co-staining, the fixed cells were incubated with an appropriate primary antibody pair as described by Field et al. (29). The slides were dried and mounted with a drop of Vectashield supplemented with 4′,6-diamidino-2-phenylindole (DAPI) (Vector Laboratories) to stain DNA. Visualization was done on a Nikon Eclipse E600 epifluorescence microscope with a Hammamatsu ORCA CCD camera and images captured using Metamorph software. Additional analysis was carried out on SP2-visible inverted confocal microscope (Leica Microsystems GmbH) and images deconvolved using Huygens Professional program (Scientific Volume Imaging). Final processing for presentation was done using Adobe Photoshop (Adobe Systems Inc.).

Primary antibodies used were mouse and rabbit anti-HA (Invitrogen; 1:1000), mouse anti-GFP (Roche), mouse anti-FLAG (Sigma), rabbit anti-TbCHC (1:250), rabbit anti-TbEpsinR (1:500), rabbit anti-Rab11 (1:200), rabbit anti-Rab5a (1:200), rabbit anti-BiP (1:1000) and mouse anti-p67 (J. Bangs, Madison, WI, USA; 1:1000). Secondary antibodies (1:1000) were anti-mouse Oregon Green/Red and anti-rabbit Oregon Green/Red (all from Molecular Probes).

Fast, isothermal fixation and electron microscopy

To avoid perturbations to endo- and exocytosis due to sample preparation, tetracycline induced and non-induced RNAi cell lines were grown to a density of 1×10^6 cells/mL and rapidly fixed in culture by the addition of isothermal glutaraldehyde to the culture flask, to a final concentration of 2.5%, as previously described (81). The culture flask was gently rocked for 10 min at 37°C, after which time fixed cells in medium were harvested by centrifugation at 800 × ***g*** for 5 min and resuspended in 2.5% glutaraldehyde in PBS for another 30 min at room temperature. Fixed cells were post-fixed in 1% osmium tetroxide in PBS for 30 min at room temperature, en bloc-stained with 1% aqueous uranyl acetate, dehydrated through acetone and embedded in epoxy resin. Ultra-thin sections (70 nm) were post-stained with 2% aqueous uranyl acetate and lead citrate. For morphometric analysis, measurements on electron micrographs were done using the publicly-available IMAGEJ software (National Institutes of Health, rsbweb.nih.gov/ij). Bar graphs and tests in Figure 9 were performed using the statistical programming package 'R' (The R Project for Statistical Computing, r-project.org).

Acknowledgments

This work was supported by the Wellcome Trust (program grant 082813 to M. C. F.), the MRC (project grant to C. G. and M. C. F.) and the Cambridge Commonwealth Trust fund (to V. O. A.). We thank Scottie Robinson, Joel Dacks and Mark Carrington for comments on the manuscript and the Cambridge Centre for Proteomics for LC–MS analysis. The authors have no conflict of interest to declare.

Supporting Information

Additional Supporting Information may be found in the online version of this article:

Figure S1: Experimental strategy. Flow chart describing the strategy designed for the identification and functional validation of TbCAPs. Black boxes denote the initial entry analysis. Green arrows and boxes denote that data met the criteria and the next set in analysis. Red specifies the criteria required for a fail and for halting the analysis. Callouts are given to the display items.

Figure S2: Immunofluorescence and co-localization of selected TbCAPs using an additional tag. A) Ectopic expression of candidates fused to a C-terminal GFP tag in pXS5 vector or endogenous-locus tagged at the C-terminus. Correct integration was confirmed by western blot or PCR. Subsequently, immunofluorescence localization of tag (green), clathrin (red) and DAPI (blue) performed. B) As in (A), but FLAG-tagged versions of selected TbCAPs were generated. C) Two TbCAP candidates that showed unexpected localizations, inconsistent with predominant clathrin interaction. The HA-tagged gene product of Tb927.5.2660 (TbCAP99) localized to the nucleus while different clones for Tb927.7.4960 (TbCAP50) showed either nuclear or endocytic region localization. TbCAP50 was also of low molecular weight, compared with the analyzed regions of the gel. These two ORFs were not pursued further. Scale bar = 2 μM.

Figure S3: Western blotting of epitope tagged TbCAPs. A) Lysate from cells expressing HA tagged TbCAPs probed with monoclonal anti-HA antibody. WT and HA-tagged ISG65 were used as negative and positive controls. B) GFP protein as a control for western blotting of GFP epitope-tagged cell lines. Note that the image is assembled from multiple blots which have been aligned for illustrative/clarity purposes only and that the background has been enhanced to make this obvious.

Figure S4: Immunofluorescence and western blot analysis of endocytic markers following knockdown of selected TbCAPs. A) Induced and non-induced RNAi lines were prepared for immunofluorescence and stained with TbCHC, TbEpsinR, TbRab5A, TbRab11 and p67. No significant localization alterations were observed on depletion of the TbCAPs. B) Total protein lysate of aliquots of induced and non-induced lines were probed for TbCHC, TbEpsinR, TbRab11 and TbRab5A. Equivalent loading was ensured by probing the same blots with anti-TbBiP. Scale bars = 2 μM.

Figure S6: Alignment of *Homo sapiens, Saccharomyces cerevisiae* and *Trypanosoma brucei* clathrin heavy chain protein sequences. The alignment was created in Clustal and is colored with fully conserved residues in red background, and conservative changes in red. Regions of conservation are boxed. ''.'' indicates gaps introduced in the alignment. Only the N-terminal 480 residues, which corresponds roughly to the β-propeller domain are shown. Amino acids contributing to binding sites mapped by Willox and Royle (94) for interacting protein partners in metazoan cells are underlined.

References

1. Mukherjee S, Ghoshi RN, Maxfield FR. Endocytosis. Physiol Rev 1997;77:759–803.
2. Nichols BJ, Lippincott-Schwartz J. Endocytosis without clathrin coat. Trends Cell Biol 2001;11:406–412.
3. Field MC, Carrington M. The trypanosome flagellar pocket. Nat Rev 2009;7:775–786.
4. Besteiro S, Dubremetz JF, Lebrun M. The moving junction of apicomplexan parasites: a key structure for invasion. Cell Microbiol 2011;13:797–805.
5. Smythe E. Clathrin-coated vesicle formation: a paradigm for coated vesicle formation. Biochem Soc Trans 2003;31:736–739.
6. Mosavi LK, Cammett TJ, Desrosiers DC, Peng Z. The ankyrin repeat as molecular architecture for protein recognition. Protein Sci 2004;13:1435–1448.
7. Edeling MA, Smoth C, Owen D. Life of a clathrin coat: insights from clathrin and AP structures. Nat Rev Mol Cell Biol 2006;7:32–44.
8. Johannes L, Lamaze C. Clathrin-dependent or not: Is it still the question? Traffic 2002;3:443–451.
9. Mayor S, Pagano RE. Pathways of clathrin-independent endocytosis. Nat Rev Mol Cell Biol 2007;8:603–612.
10. Field MC, Gabernet-Castello C, Dacks JB. Reconstructing the evolution of the endocytic system: insights from genomics and molecular cell biology. Adv Exp Med Biol 2007;607:84–96.
11. Pays E, Vanhamme L, Pérez-Morga D. Antigenic variation in *Trypanosoma brucei*: facts, challenges and mysteries. Curr Opin Microbiol 1994;7:369–374.
12. Matthews KR. The developmental cell biology of *Trypanosoma brucei*. J Cell Sci 2005;118:283–290.
13. Roditi I, Furger A, Ruepp S, Schürch N, Bütikofer P. Unravelling the procyclin coat of *Trypanosoma brucei*. Mol Biochem Parasitol 1998;91:117–130.
14. Engstler M, Pfohl T, Herminghaus S, Boshart M, Wiegertjes G, Heddergott N, Overath P. Hydrodynamic flow-mediated protein sorting on the cell surface of trypanosomes. Cell 2007;131:505–515.
15. Chung WL, Leung KF, Carrington M, Field MC. Ubiquitylation is required for degradation of transmembrane surface proteins in trypanosomes. Traffic 2008;9:1681–97.
16. Allen CL, Goulding D, Field MC. Clathrin-mediated endocytosis is essential in *Trypanosoma brucei*. EMBO J 2003;22:4991–5002.
17. Manna P, Kelly S, Field MC. Co-evolution of antigenic variation and adaptins in trypanosomatids. Mol Protein Evol 2013; (In press).
18. Pal A, Hall BS, Nesbeth DN, Field HI, Field MC. Differential endocytic functions of *Trypanosoma brucei* Rab5 isoforms reveal a glycosylphosphatidylinositol-specific endosomal pathway. J Biol Chem 2002;273:32102–32110.
19. Pal A, Hall BS, Jeffries TR, Field MC. Rab5 and Rab11 mediate transferrin and anti-variant surface glycoprotein antibody recycling in *Trypanosoma brucei*. Biochem J 2003;374:443–451.
20. Hall B, Allen CL, Goulding D, Field MC. Both of the Rab5 subfamily GTPases of *Trypanosoma brucei* are essential and required for endocytosis. Mol Biochem Parasitol 2004;138:67–77.
21. Hall BS, Pal A, Goulding D, Field MC. Rab4 is an essential regulator of lysosomal trafficking in trypanosomes. J Biol Chem 2004;279:45047–45056.
22. Hall BS, Smith E, Langer W, Jacobs LA, Goulding D, Field MC. Developmental variation in Rab11-dependent trafficking in *Trypanosoma brucei*. Eukaryot Cell 2005;4:491–980.
23. Price HP, Stark M, Smith DF. *Trypanosoma brucei* ARF1 plays a central role in endocytosis and Golgi-lysosome trafficking. Mol Biol Cell 2007;18:864–873.
24. Grünfelder CG, Engstker M, Weise F, Schwarz H, Stierhof Y, Morgan GW, Field MC, Overath P. Endocytosis of a glycosylphophatidylinositol-anchored protein via clathrin-coated vesicle, sorting by default in the endosome and exocytosis via Rab11-positive carriers. Mol Biol Cell 2003;14:2029–2040.
25. Garcia-Sacedo JA, Pérez-Morga D, Gíjón P, Dilbeck V, Pays E, Nolan DP. A differential role for actin during the life cycle of *Trypanosoma brucei*. EMBO J 2004;23:780–789.
26. Spitznagel D, O'Rourke J, Leddy N, Hanrahan O, Nolan DP. Identification and characterization of an unusual class I myosin involved in vesicle traffic in *Trypanosoma brucei*. PLoS One 2010;5:e12282.
27. Leung KF, Riley FS, Carrington M, Field MC. Ubiquitylation and developmental regulation of invariant surface protein expression in trypanosomes. Eukaryot Cell 2011;10:916–931.
28. Morgan GW, Goulding D, Field MC. The single dynamin-like protein of *Trypanosoma brucei* regulates mitochondrial division and is not required for endocytosis. J Biol Chem 2004;279:10692–10701.
29. Field MC, Lumb JH, Adung'a VO, Jones NG, Engstler M. Macromolecular trafficking and immune evasion in African trypanosomes. Int Rev Cell Mol Biol 2009;278:1–67.
30. Gabernet-Castello C, Dacks JB, Field MC. The single ENTH-domain protein of trypanosomes; endocytic functions and evolutionary relationship with epsin. Traffic 2009;107:894–911.
31. Overath P, Engstler M. Endocytosis, membrane recycling and sorting of GPI-anchored proteins: *Trypanosoma brucei* as a model system. Mol Microbiol 2004;53:735–744.
32. Engstler M, Thilo L, Weise F, Grunfelder C, Schwar H, Boshart M. Kinetics of endocytosis and recycling of the GPI-anchored variant surface glycoprotein in *Trypanosoma brucei*. J Cell Sci 2004;17:1105–1115.
33. Kabiri M, Steverding D. Studies on the recycling of the transferrin receptor in *Trypanosoma brucei* using inducible gene expression system. Eur J Biochem 2000;267:3309–3314.
34. Liu J, Qiao X, Du D, Lee MG. Receptor-mediated endocytosis in the procyclic form *Trypanosoma brucei*. J Biol Chem 2000;275:12032–12040.
35. Morgan GW, Allen CL, Jeffries TR, Hollinshead M, Field MC. Developmental and morphological regulation of clathrin-mediated endocytosis in *Trypanosoma brucei*. J Cell Sci 2001;114:2605–2615.

36. Frearson JA, Brand S, McElroy SP, Cleghorn LA, Smid O, Stojanovski L, Price HP, Guther ML, Torrie LS, Robinson DA, Hallyburton I, Mpamhanga CP, Branningan JA, Wilkison AJ, Hodgkinson M, et al. *N*-myristoyltransferase inhibitors as new leads to treat sleeping sickness. Nature 2010;464:728–732.
37. Borner GH, Harbour M, Hester S, Lilley KS, Robinson MS. Comparative proteomics of clathrin-coated vesicles. J Cell Biol 2006;175:571–8.
38. Natesan SKA, Peacock L, Matthews K, Gibson W, Field MC. Activation of endocytosis as an adaptation to the mammalian host by trypanosomes. Eukaryot Cell 2007;6:2029–2037.
39. Pearse BM. Clathrin: a unique protein associated with intracellular transfer of membrane by coated vesicles. Proc Natl Acad Sci USA 1976;73:1255–1259.
40. deGrasse JA, DuBois KN, Devos D, Siegel TN, Sali A, Field MC, Rout MP, Chait BT. Evidence for a shared nuclear pore architecture that is conserved from the last common eukaryotic ancestor. Mol Cell Proteomics 2009;8:2119–30.
41. Koumandou VL, Boehm C, Horder KA, Field MC. Evidence for recycling of invariant surface *trans*-membrane domain proteins in African trypanosomes. Cell 2013; (In press).
42. Barquilla A, Crespo JL, Navarro M. Rapamycin inhibits trypanosome cell growth by preventing TOR complex 2 formation. Proc Natl Acad Sci USA 2008;105:14579–14584.
43. de Jesus TSL, Tonelli RR, Nardelli SC, Augusto LS, Motta MCM, Girard-Dias W, Miranda K, Ulrich P, Jimenez V, Barquilla A, Navarro M, Docampo R, Schenkman S. Target of rapamycin (TOR)-like 1 kinase is involved in the control of polyphosphate levels and acidocalcisome maintaince in *Trypanosoma brucei*. J Biol Chem 2010;285:24131–40.
44. Wickstead B, Gull K. A ''holistic'' kinesin phylogeny reveals new kinesin families and predicts protein functions. Mol Biol Cell 2006;17:1734–1743.
45. Wickstead B, Gull K, Richards TA. Patterns of kinesin evolution reveal a complex ancestral eukaryote with a multifunctional cytoskeleton. BMC Evol Biol 2010;10:110.
46. Wickstead B, Gull K. Dyneins across eukaryotes: a comparative genomic analysis. Traffic 2007;8:1708–1721.
47. Maro B, Johnson MH, Pickering SJ, Louvard D. Changes in the distribution of membranous organelles during mouse early development. J Embryol Exp Morphol 1985;90:287–309.
48. Mack GJ, Compton DA. Analysis of mitotic microtubule-associated proteins using mass spectrometry identifies astrin, a spindle-associated protein. Proc Nat Acad Sci USA 2001;98:14434–14439.
49. Sogin ML, Gunderson JH, Elwood HJ, Alonso RA, Peattie DA. Phylogenetic meaning of the kingdom concept: an unusual ribosomal RNA from *Giardia lamblia*. Science 1989;243:75–77.
50. Dacks JB, Doolittle WF. Reconstructing/deconstructing the earliest eukaryotes: how comparative genomics can help. Cell 2001;107:419–425.
51. Cavalier-Smith T. Kingdoms protozoa and chromista and the eozoan root of the eukaryotic tree. Biol Lett 2010;6:342–345.
52. Altschul SF, Gish W, Miller W, Myers EW, Lipman DJ. Basic local alignment search tool. J Mol Biol 1990;215:403–410.
53. Altschul SF, Madden TL, Schäffer AA, Zhang J, Zhang Z, Miller W, Lipman DJ. Gapped BLAST and PSI-BLAST: a new generation of protein database search programs. Nucleic Acids Res 1997;25:3389–3402.
54. Eddy SR. Profile hidden Markov models. Bioinformatics 1998;14:755–763.
55. Larkin MA, Blackshields G, Brown NP, Chenna R, McGettigan PA, McWilliam H, Valentin F, Wallace IM, Wilm A, Lopez R, Thompson JD, Gibson TJ, Higgins DG, Clustal W, Clustal X. version 2.0. Bioinformatics 2007;23:2947–2948.
56. Gupta RS, Singh B. Phylogenetic analysis of 70 kD heat shock protein sequences suggest a chimeric origin for the eukaryotic cell nucleus. Curr Biol 2004;4:1104–1114.
57. Serfontein J, Nisbet RE, Howe CJ, de Vries PJ. Evolution of the TSC1/TSC2-TOR signaling pathway. Sci Signal 2010;3:ra49.
58. Foth BJ, Goedecke MC, Soldati D. New insights into myosin evolution and classification. Proc Natl Acad Sci USA 2006;103:3681–3686.
59. Katta SS, Sahasrabuddhe AA, Gupta CM. Flagellar localization of a novel myosin XXI, in *Leishmania*. Mol Biochem Parasitol 2009;164:105–110.
60. Thompson RF, Langford GM. Myosin superfamily evolution history. Anat Rec 2002;268:276–289.
61. Odronitz F, Kollmar M. Drawing the tree of eukaryotic life based on the analysis of 2,269 manually annotated myosins from 328 species. Genome Biol 2007;8:R196.
62. Pérez-Victoria FJ, Schindler C, Magadán JG, Mardones GA, Delevoye D, Romao M, Raposo G, Bonifacino J. Ang2/Fat-free is a conserved subunit of the Golgi-associated retrograde protein complex. Mol Biol Cell 2010;21:3386–3395.
63. Koumandou VL, Dacks JB, Coulson RMR, Field MC. Control systems for membrane fusion in the ancestral eukaryote; evolution of tethering complexes and SM proteins. BMC Evol Biol 2007;7:29.
64. Kim E, Sheng M. PDZ domain proteins of synapses. Nat Rev 2004;5:771–781.
65. Gomperts SN. Clustering membrane proteins: it's all coming together with the PSD-95/SAP90 protein family. Cell 1996;84:659–662.
66. Fanning AS, Anderson JM. Protein modules as organizers of membrane structure. Curr Opin Cell Biol 1999;11:432–439.
67. Komachi K, Redd MJ, Johnson AD. The WD repeats of Tup1 interact with the homeo domain protein alpha 2. Gene Dev 1994;8:2857–2867.
68. Neer EJ, Schmidt CJ, Nambudripad R, Smith TF. The ancient regulatory-protein family WD-repeat proteins. Nature 1994;371:297–300.
69. Michaely P, Kamal A, Anderson RGW, Bennett V. A requirement for ankyrin binding to clathrin during coated pit budding. J Biol Chem 1999;274:35908–35913.
70. Li J, Mahajan A, Tsai M. Ankyrin repeat: a unique motif mediating protein–protein interactions. Biochemistry 2006;45:15168–15178.
71. Rubstov AM, Lopina OD. Ankyrins. FEBS Lett 2000;482:1–5.
72. Cunha SR, Mohler PJ. Ankyrin protein networks in membrane formation and stabilization. J Cell Mol Med 2009;13:4364–76.
73. Koumandou VL, Natesan SK, Sergeenko T, Field MC. The trypanosome transcriptome is remodeled during differentiation but displays limited responsiveness within life stages. BMC Genomics 2008;9:298.
74. Balber AE, Frommel TO. *Trypanosoma brucei gambiense* and *T. b. rhodesiense*: concanavalin A binding to the membrane and flagellar pocket of bloodstream and procyclic forms. J Protozool 1988;35:214–219.
75. Brickman MJ, Cook JM, Balber AE. Low temperature reversibly inhibits transport from tubular endosomes to a perinuclear, acidic compartment in African trypanosomes. J Cell Sci 1995;108:3611–21.
76. Hoock TC, Peters LL, Lux SE. Isoforms of ankyrin-3 that lack the NH2-terminal repeats associate with mouse macrophage lysosomes. J Cell Biol 1997;136:1059–1070.
77. Ignatiuk A, Quickfall JP, Hawrysh AD, Chamberlain MD, Anderson DH. The smaller isoforms of ankyrin 3 bind to the p58 subunit of phosphatidylinositol 3′-kinase and enhance platetet-derived growth factor receptor down-regulation. J Biol Chem 2006;281:5956–5964.
78. Devarajan P, Stabach P, Mann A, Ardito T, Kashgarian M, Morrow J. Identification of a small cytoplasmic ankyrin (AnkG119) in the kidney and muscle that binds BIE spectrin and associates with the Golgi apparatus. J Cell Sci 1996;133:819–830.
79. Beck KA, Buchanan JA, Nelson WJ. Golgi membrane skeleton: identification, localization and oligomerization of a 195 kDa ankyrin isoform associated with the Golgi complex. J Cell Sci 1997;110:1239–1249.
80. Lacomble S, Vaughan S, Gadelha C, Morphew MK, Shaw MK, Mcintosh JR, Gull K. Three-dimensional cellular architecture of the flagellar pocket and associated cytoskeleton in trypanosomes revealed by electron microscope tomography. J Cell Sci 2009;122: 1081–1090.
81. Gadelha C, Rothery S, Morphew M, Mcintosh JR, Severs NJ, Gull K. Membrane domains and flagellar pocket boundaries are influenced by the cytoskeleton in African trypanosomes. Proc Natl Acad Sci USA 2009;106:17425–17430.
82. Saffarian S, Cocucci E, Kirchhausen T. Distinct dynamics of endocytic clathrin-coated pits and coated plaques. PLoS Biol 2009;7:e1000191.
83. Taylor MJ, Perrais D, Merrifield CJ. A high precision survey of the molecular dynamics of mammalian clathrin-mediated endocytosis. PLoS Biol 2011;9:e1000604.

84. Devos D, Dokudovskaya S, Williams R, Alber F, Eswar N, Chait BT, Rout MP, Sali A. Simple fold composition and modular architecture of the nuclear pore complex. Proc Natl Acad Sci USA 2006;103:2172–2177.
85. Field MC, Sali A, Rout MP. On a bender: Bars, ESCRTs, COPs and finally getting your coat. J Cell Biol 2011;193:963–972.
86. Field MC, Dacks JB. First and last ancestors; reconstructing evolution of the endomembrane system with ESCRTs, vesicle coat proteins, nuclear pore complexes. Curr Opin Cell Biol 2009;21:4–13.
87. Elias M, Brighouse A, Castello CG, Field MC, Dacks JB. Sculpting the endomembrane system in deep time: High resolution phylogenetics of Rab GTPases. J Cell Sci 2012;125:2500–2508.
88. Hansen CG, Nichols BJ. Molecular mechanisms of clathrin-independent endocytosis. J Cell Sci 2009;122:1713–1721.
89. Traub LM. Regarding the amazing choreography of clathrin coats. PLoS Biol 2011;9:e1001037.
90. Kirchhausen T. Imaging endocytic clathrin structures in living cells. Trends Cell Biol 2009;19:596–605.
91. Kukulski W, Schorb M, Kaksonen M, Briggs JA. Plasma membrane reshaping during endocytosis is revealed by time-resolved electron tomography. Cell 2012;150:508–20.
92. den Otter WK, Briels WJ. The generation of curved clathrin coats from flat plaques. Traffic 2011;12:1407–16.
93. Broadhead R, Dawe HR, Farr H, Griffiths S, Hart SR, Portman N, Shaw MK, Ginger ML, Gaskell SJ, McKean PG, Gull K. Flagellar motility is required for the viability of the bloodstream trypanosome. Nature 2006;440:224–7.
94. Willox AK, Royle SJ. Functional analysis of interaction sites on the N-terminal domain of clathrin heavy chain. Traffic 2012;13:70–81.
95. Berriman M, Ghedin E, Hertz-Fowler C, Blandin G, Renauld H, Bartholomeu CD, Lennard NJ, Caler E, Hamlin NE, Haas B, Böhme U, Hannick L, Aslett MA, Shallom J, Marcello L, et al. The genome of the African trypanosome *Trypanosoma brucei*. Science 2005;309:416–422.
96. Michaels PA, Bringaud F, Herman M, Hannaert V. Metabolic functions of glycosomes in trypanosomatids. Biochim Biophys Acta 2006;1763:1463–77.
97. Wirtz E, Leal S, Ochatt C, Cross GA. A tightly regulated inducible expression system for conditional gene knock-outs and dominant-negative genetics in *Trypanosoma brucei*. Mol Biochem Parasitol 1999;99:89–102.
98. O'Reilly AJ, Dacks JB, Field MC. Evolution of the karyopherin-β family of nucleocytoplasmic transport factors; ancient origins and continued specialization. PLoS One 2011;6:e19308.
99. Finn RD, Mistry J, Tate J, Coggill P, Heger A, Pollington JE, Gavin OL, Gunasekaran P, Ceric G, Forslund K, Holm L, Sonnhammer ELL, Eddy SR, Bateman A. The Pfam protein families database. Nucleic Acids Res 2010;38:D211–D222.
100. Hunter S, Apweiler R, Attwood TK, Bairoch A, Bateman A, Binns D, Bork P, Das U, Daugherty L, Duquenne L, Finn RD, Gough J, Haft D, Hulo N, Kahn D, et al. InterPro: the integrative protein signature database. Nucleic Acids Res 2009;37:D211–D215.
101. Sigrist CJA, Cerutti L, de Castro E, Langendijk-Genevaux PS, Bulliard V, Bairoch A, Hulo N. PROSITE, a protein domain database for functional characterization and annotation. Nucleic Acids Res 2010;38:D161–D166.
102. Redmond S, Vadivelu J, Field MC. RNAit: an automated web-based tool for the selection of RNAi targets in *Trypanosoma brucei*. Mol Biochem Parasitol 2003;128:115–118.
103. Alibu VP, Storm L, Haile S, Clayton C, Horn D. A doubly inducible system for RNA interference and rapid RNAi plasmid construction in *Trypanosoma brucei*. Mol Biochem Parasitol 2005;139:75–82.
104. Oberholzer O, Morand S, Kunz S, Seebeck T. A vector series for rapid PCR-mediated C-terminal in situ tagging of *Trypanosoma brucei* genes. Mol Biochem Parasitol 2006;145:117–120.
105. Jeffries TR, Morgan GW, Field MC. A developmentally regulated Rab11 homogue in *Trypanosoma brucei* is involved in recycling process. J Cell Sci 2001;114:2617–2626.
106. Bangs JD, Uyetake L, Brickman MJ, Balber AE, Boothroyd JC. Molecular cloning and cellular localization of a BiP homologue in *Trypanosoma brucei*. Divergent ER retention signals in a lower eukaryote. J Cell Sci 1993;105:1101–1113.